International Journal of Biological Macromolecules 265 (2024) 131025

Contents lists available at ScienceDirect

International Journal of Biological Macromolecules

journal homepage: www.elsevier.com/locate/ijbiomac

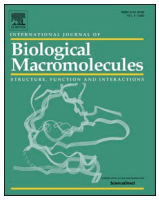

Unzipped carbon nanotubes assisted 3D printable functionalized chitosan hydrogels for strain sensing applications

Dinesh K. Patel [a], So-Yeon Won [a], Tejal V. Patil [b], Sayan Deb Dutta [b], Ki-Taek Lim [b,*], Sung Soo Han [a,*]

[a] School of Chemical Engineering, Yeungnam University, 280-Daehak-ro, Gyeongsan 38541, Republic of Korea
[b] Department of Biosystems Engineering, Institute of Forest Science, Kangwon National University, Chuncheon 24341, Republic of Korea

ARTICLE INFO

Keywords:
Carboxymethyl chitosan
Unzipped CNTs
Adhesiveness
Biocompatibility
Strain-sensing

ABSTRACT

Developing multifunctional hydrogels for wearable strain sensors has received significant attention due to their diverse applications, including human motion detection, personalized healthcare, soft robotics, and human-machine interfaces. However, integrating the required characteristics into one component remains challenging. To overcome these limitations, we synthesized multifunctional hydrogels using carboxymethyl chitosan (CMCS) and unzipped carbon nanotubes (f-CNTs) as strain sensor *via* a one-pot strategy. The polar groups in CMCS and f-CNTs enhance the properties of the hydrogels through different interactions. The hydrogels show superior printability with a uniformity factor (U) of 0.996 ± 0.049, close to 1. The f-CNTs-assisted hydrogels showed improved storage modulus (8.8×10^5 Pa) than the pure polymer hydrogel. The hydrogels adequately adhered to different surfaces, including human skin, plastic, plastic/glass interfaces, and printed polymers.

The hydrogels demonstrated rapid self-healing and good conductivity. The biocompatibility of the hydrogels was assessed using human fibroblast cells. No adverse effects were observed with hydrogels, showing their biocompatibility. Furthermore, hydrogels exhibited antibacterial potential against *Escherichia coli*. The developed hydrogel exhibited unidirectional motion and complex letter recognition potential with a strain sensitivity of 2.4 at 210 % strain. The developed hydrogels could explore developing wearable electronic devices for detecting human motion.

1. Introduction

The demand for smart wearable electronic devices to monitor human motion and personalized healthcare issues globally is rapidly increasing. Different characteristics, including conductivity, adhesiveness, biocompatibility, and sensitivity, are required in developing wearable electronic devices [1–3]. However, integrating these required properties into one component remains challenging. Metals and semiconductors-based wearable electronic devices exhibited better sensitivity than other developed materials. However, their broad applicability is restricted under adverse conditions due to their poor mechanical strength, where any minor deformations cause adverse effects on their sensitivity [4,5]. Therefore, materials that promptly recover their initial characteristics are highly desirable in developing wearable electronic devices for different applications. Conductive polymer-based hydrogels are attractive platforms for developing wearable electronic devices owing to their superior conductivity, biocompatibility, and sensitivity [6]. The broad applicability of the conductive polymer-based hydrogels for strain sensing applications is also limited owing to their low stretchability and high hysteresis [7]. Song and coworkers developed hysteresis-free and stretchable conductive hydrogels for strain-sensing applications. However, their developed devices typically had low strain sensitivity [8]. Therefore, developing biocompatible conductive hydrogels without using conductive polymers with good strain sensitivity is required for human motion sensing applications.

Adhesive hydrogels have received considerable significance in developing wearable electronic devices for diverse applications because they do not require additional tapes or bandages for the adhesion on the applied surfaces, which may cause skin irritation or infections [9,10]. The dopamine or tannic acid-based hydrogels exhibited enhanced adhesiveness due to highly reactive catechol functional groups in their structures. However, they need further functionalization or conductive materials to improve the conductivity of the developed hydrogels [11,12]. Qu and coworkers developed skin-inspired, highly stretchable,

* Corresponding authors.
E-mail addresses: ktlim@kangwon.ac.kr (K.-T. Lim), sshan@yu.ac.kr (S.S. Han).

https://doi.org/10.1016/j.ijbiomac.2024.131025
Received 4 January 2024; Received in revised form 15 March 2024; Accepted 18 March 2024
Available online 20 March 2024

and conductive hydrogels using cellulose nanofibrils modified tannic acid for strain sensing applications. The developed hydrogels showed moderate adhesiveness to different surfaces, including human skin, plastic, rubber, and metals [13]. Three-dimensional (3D) printable hydrogels have additional advantages over conventional hydrogels owing to their printability characteristics in the desired shape and size [14].

Biocompatibility is also essential in developing wearable electronic devices for strain-sensing applications. Various polymers, including chitosan, sodium alginate, polyvinyl alcohol, carboxymethyl cellulose, and polyurethanes, have been explored for sensing applications due to their remarkable biocompatibility [15–17]. Chitosan (CS) has received significant interest in developing wearable devices due to its superior biocompatibility and antibacterial characteristics [18]. The abundant hydroxyl and amine in the CS backbone facilitate the formation of physically and chemically cross-linked hydrogels for different applications [19]. The antibacterial potential provides an additional advantage in developing wearable electronic devices, which restricts the growth of bacterial infection for long-term applicability [20]. However, the weak mechanical strength limits the broad applicability of chitosan. This limitation can be overcome by adding other suitable polymers or nanomaterials. The mechanical stability of functionalized CS can also be improved by cross-linking with diverse metal ions for the desired applications [21]. Yan and coworkers synthesized sodium alginate and carboxymethyl chitosan-based hydrogels cross-linked with ions, such as Ca^{2+}, Zn^{2+}, Fe^{3+}, Ni^{2+}, Ag^{+}, and Co^{2+} for bacterial detection and sterilization. The metallohydrogels demonstrated improved mechanical stability and fluorescent characteristics [22]. Different nanomaterials, such as carbon nanotubes (CNTs), nanocellulose, reduced graphene oxide, and clay, are widely explored to enhance the mechanical strength of native polymers [23–26]. Multi-walled or single-walled CNTs are often explored in developing wearable electronic devices for strain-sensing applications owing to their appealing properties, such as high electrical conductivity, good structural stability, superior mechanical strength, and tunable surface chemistry [27–29]. However, their better dispersion remains challenging in the polymer matrices due to their hydrophobic characteristics, causing catastrophic effects on the polymer properties [30]. Therefore, better dispersion of CNTs is necessary to enhance the properties of polymers. Different approaches, including surface functionalization and surfactants, are used to improve the dispersion of CNTs in the polymer matrix [23]. Qin and coworkers used amphiphilic sodium dodecyl sulfate to improve the dispersion of hydrophobic CNTs in polyacrylamide hydrogels for sensing applications [31]. The unzipping approach facilitates the addition of different functional groups on the surface of CNTs, aiding in better dispersion. The unzipping also increases the surface area while maintaining the original characteristics of CNTs [32].

Herein, we developed 3D-printable and multifunctional hydrogels of functionalized chitosan/f-CNTs *via* a one-pot synthesis approach without using any surfactants for strain sensing applications. The developed hydrogels were characterized by different spectroscopic techniques, including Fourier transform infrared spectroscopy (FTIR), X-ray diffraction (XRD), scanning electron microscopy (SEM), and rheometer. The developed hydrogels have no adverse effects on human dermal fibroblasts (HDFs) and also exhibit antibacterial potential. The motion sensing potential of the developed hydrogels was monitored at different human body parts, including finger, wrist, and elbow. The hydrogels also demonstrated the completed letter sensing potential. Taken together, we hypothesized that the developed hydrogels have the potential to develop wearable electronic devices for monitoring human motion as well as in personalized healthcare sectors.

2. Experimental section

2.1. Materials

The high molecular weight chitosan (CS) powder (MW:310–375 kDa, Deacetylated chitin: >75 %), sodium hydroxide (Junsei Chemicals, Japan), isopropanol (Thermo Fischer Scientific), monochloroacetic acid (Duksan Chemicals, Republic of Korea), hydrochloric acid (35 %), sulfuric acid (95 %), hydrogen peroxide (35 %) (mass/mass, Wako Chemicals, Republic of Korea), potassium permanganate (Daejung Chemicals, Republic of Korea), and sodium nitrate (Sigma-Aldrich, USA) were used as received from the suppliers in this work.

2.2. Synthesis of functionalized chitosan

The synthesis of water-soluble carboxymethyl functionalized chitosan (CMCS) was performed as earlier reported somewhere else with some modifications [33]. In Brief, the required amounts of CS (10 g) were added into 50 % (w/v) sodium hydroxide solution and mixed well. The mixture was kept in the refrigerator at 4 °C for 24 h. Then, the calculated amounts (200 mL) of isopropanol were added with continuous mechanical stirring for 30 min. After that, the required amounts of monochloroacetic acid (15.0 g) were added to the reaction mixture. The reaction mixture was heated to 60 °C for 6 h with continuous mechanical stirring. Then, the reaction mixture was filtered and washed with ethanol three times to remove the unreacted chemical reagents. The filtrate sample was dissolved in distilled water and dialyzed for 4 days, followed by the performing the rotary evaporation process to concentrate the solution and freeze-drying by freeze dryer (EYELA® Freeze Drying Unit 2200, Tokyo, Japan).

2.3. Unzipping of carbon nanotubes (f-CNTs)

CNTs were unzipped in our previously reported work [32]. Briefly, the known amount (1 g) of multi-walled carbon nanotubes (MWCNTs) was added into 100 mL sulfuric acid solution with continuous mechanical stirring at room temperature. After that, 10 g sodium nitrate was added to the reaction mixture and stirred for 2 h, followed by slowly adding 5 g potassium permanganate powders. The reaction mixture temperature was increased to 70 °C and stirred for another 2 h, followed by the addition of hydrogen peroxide solution to overcome insoluble manganese oxide precipitation. After that, the reaction mixture was filtered and repeatedly washed with distilled water until the solution became neutral. The obtained sample was dried in an air oven at 50 °C for 2 days. The f-CNTs in this work indicated the prepared material.

2.4. Synthesis of 3D-printable conductive hydrogels

The pure polymer hydrogel was developed by adding the calculated amounts (5 %, w/v) of carboxymethyl chitosan (CMCS) in distilled water. The composite hydrogels were developed by incorporating different amounts of f-CNTs (1, 2, and 4 wt%, w.r.t. to the CMCS weights) in the polymer matrix. The prepared hydrogels were transferred into different molds and kept at 4 °C for 12 h, followed by −20 °C for 4 h. The hydrogels were unfrozen at room temperature for 6 h. This process was repeated 3 times to achieve a more compact structure. The frozen and unfrozen processes were performed as reported elsewhere to develop compact hydrogels with a greater interaction [34]. The developed hydrogels were indicated by CMCS, and CMCS/f-CNTs-x. Where x is the amount of f-CNTs in the polymer matrix.

2.5. Spectroscopic characterizations of hydrogels

Fourier transform infrared (FTIR) spectroscopy (Frontier, Perkin Elmer, UK) was used to examine the interactions between the CMCS matrix and f-CNTs in the 4000–400 cm^{-1} range with a resolution of 4 cm^{-1}. The number of measured scans was 36 in the FTIR analysis. The structural changes in the hydrogel films were assessed by X-ray diffractometer (X'Pert PRO MPD, Philips, Eindhoven, Netherlands) at the operating voltage and current of 40 kV and 40 mA, with Cu Kα radiation (λ = 1.5414 A°). The operating range (2θ) was 5–40°. The surface morphologies of the hydrogel scaffolds were examined by field emission scanning electron microscopy (FE-SEM) (TESCAN, Czech Republic). Before the SEM analysis, the hydrogels were freeze-dried using a freeze-dryer for 3 days, and coated with platinum for 100 s. The image J (NIH) software was used to determine the pore diameter of the hydrogel's scaffolds. The rheological characteristics of the hydrogels were assessed by an ARES-G2 rheometer (TA Instrument, New Castle, Delaware, USA) with a 6 mm parallel plate at 37 °C. The tensile strength of the hydrogel films (dry conditions) was assessed using a universal testing machine (UTM) (MCT-1150, A&D, Co. Japan) with an elongation speed of 10.0 mm/min. The mechanical strength of the hydrogels was also measured in compression mode with a compression speed of 10.0 mm/min.

2.6. 3D-printing of hydrogels

The pre-designed 3D structures were constructed on a sterile petri dish using the CELLINK BIO-X printer. The design of the 3D constructs was developed by the SolidWorks software (www.solidworks.com, Dassault Biosystems, France). The rectangular (20 × 20 × 2 mm^3) constructs were printed on the plate using a needle (22G). The printing speed and pressure were 2 mm/s and 90–120 kPa, respectively. The printing process was performed at room temperature. The printability of the developed hydrogels was determined in terms of the uniformity factor (U), expansion ratio (α), and pore factor (Pr) by using the equations given below,

$$Uniformity\ factor\ (U) = \frac{\text{Length of the 3D printed strand (l)}}{\text{Length of the theoretical design (L)}}$$

$$Expansion\ ratio\ (\alpha) = \frac{\text{Diameter of the 3D printed strand (d)}}{\text{Diameter of the nozzle (D)}}$$

$$Pore\ factor\ (Pr) = \frac{(\text{Pore perimeter})^2}{(16 \times \text{pore area})}$$

The five pores (perimeter and pore area) were measured for each printed scaffold. Depending upon the pore factor value (<1, >1, or =1), gels were classified as under-gelled, over-gelled, or properly gelled, respectively [35].

2.7. Recovery, self-healing, and adhesiveness examination

The recovery potential of the hydrogels was monitored in terms of the viscosity changes under different shear rates (0.1, 100, and 0.1 s^{-1}) for different intervals (0–100, 101–200, and 201–300 s) at 25 °C, respectively. The change in the viscosity was measured using an ARES-G2 rheometer with a 6 mm parallel plate. The self-healing ability of the hydrogels was examined by cutting and re-joining methods at room temperature without the influence of external factors, including temperature, pH, and pressure. In brief, a defined dimension of the hydrogel was cut into two halves and placed together to re-join after some intervals. After re-joining, the hydrogel was lifted with forceps to validate the healing process. The quantitative self-healing efficiency of the hydrogels (original and self-healed) was also assessed through the rheometer. The following equation was used to measure the self-healing potential of the hydrogels.

$$\%Self-healing\ efficiency = \frac{\text{Storage modulus of orignial hydrogel}}{\text{Storage modulus of healed hydrogel}} \times 100$$

The adhesive strength of the hydrogels was assessed as reported earlier somewhere else [36]. In brief, 150 mg hydrogels were placed on a thick paper surface and spread over an area of 15 mm × 15 mm. After that, the second paper was kept on the hydrogel surface and left for 15 min at room temperature. The adhesive strength of the developed hydrogels was measured using a uniaxial tensile machine. All experiments were completed in triplicate ($n = 3$).

2.8. Biocompatibility assessment

2.8.1. Primary cell culture

The human fibroblast (HDF) cells were received from the Korean Cell Line Bank (KCLB, Seoul, Republic of Korea). Cell cultured was accomplished, as previously reported somewhere, using Dulbecco's modified Eagle medium (DMEM; Welgene Inc., Republic of Korea) containing 10 % fetal bovine serum (FBS; Welgene Inc., Republic of Korea), and 1 % antibiotic-antimycotic (Anti-Anti; 100×, Gibco, USA) in a 5 % CO_2 incubator (Steri-Cycle 370 Incubator; Thermo-Fischer Scientific, USA) at 37 °C [37]. The old cultured media were replaced with the fresh culture media after 3 days of interval. After ~80 % of confluency, the cells were washed with PBS (3 times), followed by the treatment with 1 mL of 0.25 % trypsin-ethylenediaminetetraacetic acid (EDTA; Gibco, USA) to detach and count the cells. Passage three was used for the cell experiment in this study.

2.8.2. Cell viability assay

The biocompatibility of the synthesized hydrogel scaffolds was assessed with HDF cells through WST-8 assay as previously reported with some modifications [38]. For this, 1 × 10^4 HDF cells/100 μL media were placed on the surface of the scaffolds in a 96-well plate and incubated in a 5 % CO_2 incubator at 37 °C for 24 h. The media without hydrogel scaffold treatment were set to be controlled. After incubation, each well was washed with PBS (3 times), and the fresh cultured media was added. After that, 10 μL of WST-8 dye was added to the cultured media and incubated for 2 h to develop the formazan. The formed formazan was collected in a new culture plate, and absorbance was recorded through a spectrophotometer at 450 nm. The absorbance at 625 nm was considered as a reference value. All experiments were done in triplicate ($n = 3$), and the results are shown as mean optical density (OD) ± standard deviations (SDs). Statistical significance was taken at $^*p < 0.05$.

2.8.3. Live-dead assay

The survivability of the cultured HDF cells on the surface of the hydrogel scaffolds was examined through live-dead fluorescence imaging. For this, cells (1 × 10^4) were seeded on the surface of the scaffolds in a 6-well plate and incubated in a 5 % CO_2 incubator at 37 °C for 24 h. The groups without scaffold treatment were taken as control. After incubation, cells were washed with PBS (3 times) and treated with 1 μL of acridine orange (AO) and ethidium bromide (EtBr) dye solution at a ratio of 1:1. After that, the images were taken using the inverted fluorescence microscope (DMi8 Series, Leica Microsystems, Germany).

2.9. Antibacterial analysis

The antibacterial potential of the developed hydrogels was assessed against *Escherichia coli* (*E. coli*; ATCC 10536) by measuring the optical density (OD) at different periods, as previously reported somewhere with some modifications [39]. The new bacterial colonies were generated by suspending the purchased bacteria in the nutrient broth under continuous stirring (150 rpm) and incubating it at 37 °C for 12 h. After that, the OD of the freshly cultured bacteria was taken using a spectrophotometer at 600 nm. The cultured bacteria were diluted 100 times.

Then, small amounts of hydrogels (7 mg/mL) were suspended in the bacterial medium and incubated for 1 and 5 h. The groups without hydrogel treatment were considered as controls. The change in OD was recorded using a spectrophotometer at 600 nm. The % growth of the bacteria was calculated using the following equation.

$$\%growth = \frac{\text{OD at measured time} - \text{OD of the cultured media at zero time}}{\text{OD at measured time}} \times 100$$

The antibacterial potential of the developed hydrogels was also monitored through colony counting methods. In brief, 100 μL of the diluted bacteria was transferred to the nutrient broth having 10 mL of cultured media with the hydrogels (~7 mg/mL) and incubated at 37 °C for 24 h. Then, 100 μL of the bacteria media was taken, spread onto agar plates, and incubated at 37 °C to generate new bacteria colonies. The groups without hydrogel treatment were considered as controls.

2.10. Electrochemical performance and sensing potential

The conductance property of the synthesized hydrogels was assessed using the Keithley 2460 source meter® at room temperature. The hydrogel dimensions are given in the Table S1. The conductance potential of the hydrogels was determined by using the equation given below,

$$Conductance\left(\frac{1}{R}\right) = \text{Slope of } \frac{\mathrm{I}}{\mathrm{V}} curve$$

The motion-sensing potential of the hydrogel was examined using an electrochemical workstation (BioLogic Science Instruments, France) at 5 V at room temperature. For this, hydrogel, a definite dimension (12.50 × 4.80 × 3.60 mm^3), was placed on different parts of the human body, including the finger, wrist, knee, and biceps, and connected with the conductive wires, which were connected to the source meter. The current changes were measured during the motion of the body parts and examined the strain-sensing ability of the hydrogels. The relative resistance change ($\Delta R/R_0$) was calculated by using the equation mentioned below.

$$Relative\ resistance\ change\left(\frac{\Delta R}{R_0}\right) = \left(\frac{R_s - R_0}{R_0}\right) \times 100$$

Here, R_0 and R_s are the hydrogel initial and deformed resistance, respectively.

The strain sensitivity of the hydrogels was assessed in terms of the gauge factor (GF) by using the equation below.

$$Gauge\ factor\ (GF) = \frac{\frac{(\Delta R)}{R_0}}{\varepsilon}$$

Here, ($\Delta R/R_0$), and ε are the hydrogel relative resistance and strain change, respectively.

To examine the multidimensional recognition ability, the hydrogels were sandwiched between two thin polyethylene films and connected to the source meter through the conductive wires. The desired letters were written to the surface of the polyethylene film, and current changes were measured. All experiments were performed in triplicate ($n = 3$), and average data were considered in the results.

2.11. Statistical analysis

Statistical analyses were performed with one-way ANOVA using Origin Pro8.5 software. The data are given as average ± standard deviations (SD). Statistical significance was taken at $^*p < 0.05$, $^{**}p < 0.01$, and $^{***}p < 0.001$. A comparison was performed between the control and experimental groups in this work.

3. Results and discussion

3.1. Interaction and structural characteristics of hydrogels

The detailed spectroscopic characterizations of f-CNTs, including FTIR, XRD, TGA, and zeta potential, are given in our previously reported work [32]. The schematic presentation for the one-pot synthesis of 3D-printable multifunctional chitosan hydrogel using f-CNTs with plausible interactions among the hydrogel's components for strain-sensing applications is presented in (Fig. 1a). The 3D-printable hydrogels were synthesized by adding the required amounts of the components in water. The detailed spectroscopic characterizations of f-CNTs have previously been reported by our group [32]. The FTIR spectra of the pure CS and functionalized CS are shown in (Fig. 1b). The characteristics absorption peaks in CS at 3330, 2910–2869, 1647, 1586, 1424, 1377, and 1319 cm^{-1} are assigned to the hydrogen-bonded –NH/–OH, $–CH_2/CH_3$ symmetric/asymmetric stretching, amide I, amide II of the residual *N*-acetyl functional groups, $–CH_2/CH_3$ bending vibration, and –CN stretching, respectively. The absorption peaks at 1148, 1063, and 1025 cm^{-1} can be attributed to the asymmetric stretching of the –C-O-C bridge and –C-O stretching. These typical peaks exist in other polysaccharides, such as xylan and glucan [40]. After functionalization, the intensity of these peaks was increased, indicating the presence of more polar functional groups. The position of hydrogen-bonded –NH/–OH, $–CH_2/CH_3$ symmetric/asymmetric stretching, amide I, and amide II of the residual *N*-acetyl functional groups was also shifted in the functionalized CS due to the change in the electronic environments. Additionally, new peaks at 1749 and 1416 cm^{-1} appeared in the functionalized CS, which are attributed to the stretching vibration of carbonyl (>C=O) and stretching vibration of $–COO^-$ functional groups of $–CH_2COOH$ moiety, showing the successful functionalization of CS to CMCS [41].

The f-CNTs and CMCS contain plenty of functional groups, including carboxylic (–COOH), hydroxyl (–OH), and amino ($–NH_2$) in their backbone. Therefore, it is anticipated that the developed hydrogels could be interactive among the functional groups. The FTIR spectroscopic analysis was performed to monitor the interactions between the hydrogel components, and the spectra are given in (Fig. 1c). It was interesting to note that these polysaccharide absorption peaks significantly shifted their positions in the composite hydrogels due to the change in the electronic environment through different interactions. A significant shifting in stretching vibration of hydrogen-bonded amine/hydroxyl groups was observed in the composite hydrogels (3324 → 3345 cm^{-1}) due to the interaction between the polar groups of the functionalized polymer chains and f-CNTs [36]. These interactions also facilitate the absorption shifting in stretching vibration of amide I (1647 → 1642 cm^{-1}), bending vibration of amide II (1578 → 1591 cm^{-1}), and carbonyl –CO/COO (1066 → 1055 cm^{-1}) functional groups. These changes suggest that the insertion of f-CNTs occurred inside the galleries of CMCS polymer chains, minimizing the strong interaction between the polymer chains and facilitating the interaction between CMCS polymer chains and f-CNTs [42]. Due to these interactions, hydrogels demonstrated improved physiochemical properties, including 3D printability, viscoelasticity, adhesiveness, and recovery potential. The hydrogels have abundant active polar functional groups and charged f-CNTs. Therefore, the secondary interactions, including dipole-dipole interaction, hydrogen bonding, and electrostatic interactions, are expected to play crucial roles in these shifts [43].

The XRD analysis assessed the influence of f-CNTs on structural changes in CMCS polymer, and the diffraction patterns are given in (Fig. 1d). The pure CMCS polymer shows two diffraction peaks at 8.1° and 21.5° with corresponding d-spacing of 1.04, and 0.42 nm, respectively, indicating the presence of some random and ordered orientation in the polymer [44]. The diffraction of the pure CMCS polymer is similar to the previously reported work [33]. The addition of f-CNTs in the polymer matrix facilitated the shifting of these peaks towards a lower angle (7.5°) while increasing the d-space value (1.18 nm),

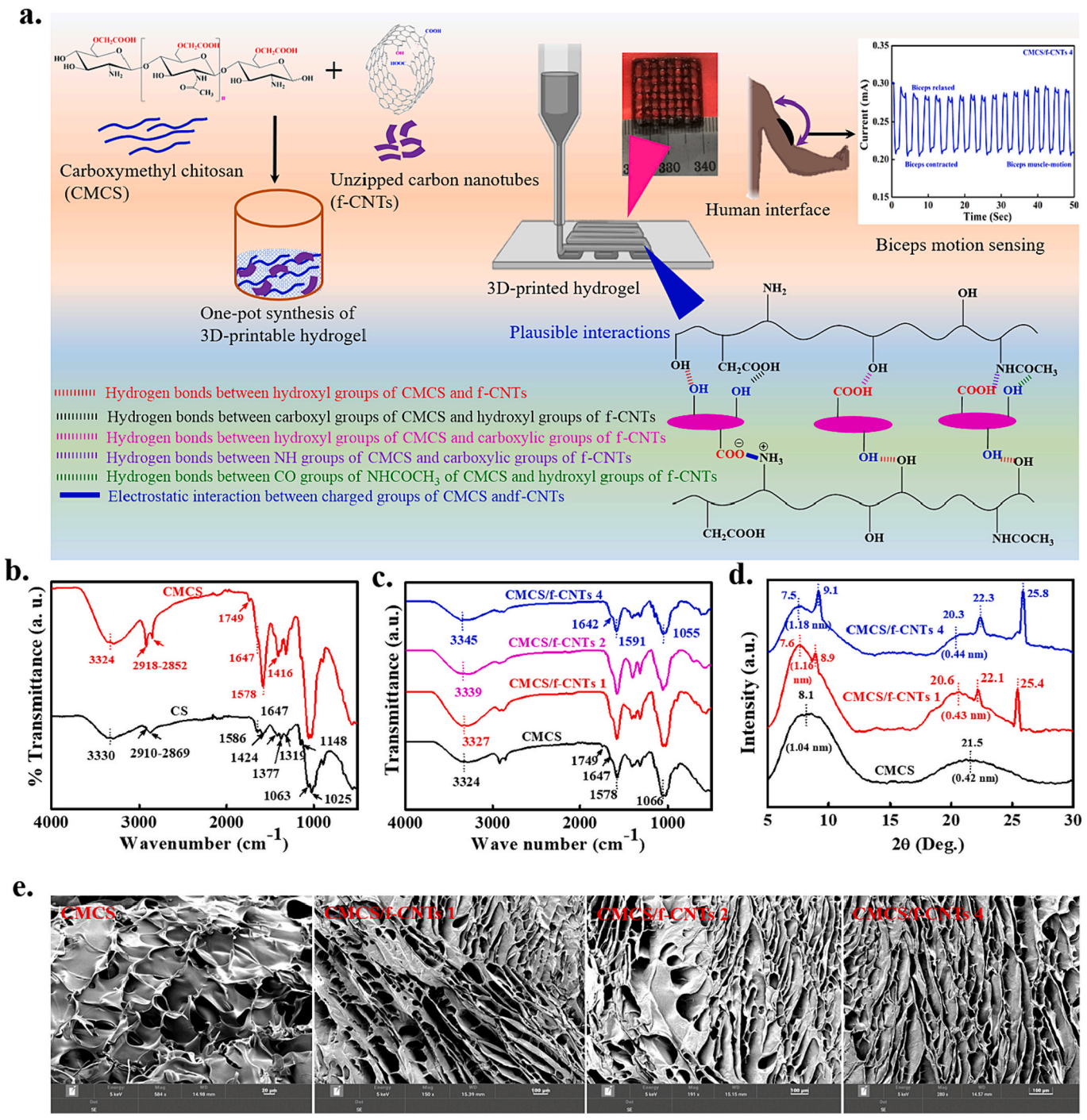

Fig. 1. (a) The schematic presentation for 3D-printable multifunctional chitosan hydrogel using f-CNTs for strain-sensing applications with plausible interactions among the hydrogel's components, (b) FTIR spectra of pure CS and CMCS, (c) FTIR spectra of CMCS and indicated composite hydrogel scaffolds, (d) XRD patterns of the indicated hydrogel scaffolds, and (e) SEM morphologies of the indicated hydrogel scaffolds.

demonstrating the successful insertion of the f-CNTs between the polymer layers. The insertion of the f-CNTs between the polymer layers improved the interactions between the added materials, as observed in FTIR results, and enhanced the properties of the developed hydrogels. Moreover, the composite hydrogels also contain other diffraction peaks at ~9.0°, 22.3°, and 25.8° attributed to f-CNTs in the polymer matrix [32]. The lower angle diffraction peak at ~9.0° indicated the presence of oxygenated moieties, whereas higher angle diffraction peaks at ~22.3° and 25.8° showed the existence of graphitic structure. The intensity of these peaks increased with an increase in the content of f-CNTs in the polymer matrix.

The surface morphology of the developed hydrogel scaffolds was examined through FE-SEM, and the morphologies are presented in (Fig. 1e). The hydrogel scaffolds show porous and interconnected morphology. The composite hydrogel scaffolds demonstrate a rough surface morphology vis-à-vis pure polymer scaffolds due to the distribution of f-CNTs in the polymer matrix. The pure polymer scaffold exhibits a randomly oriented morphology, whereas an aligned morphology was observed in the composite scaffolds. The aligned morphology in the composite scaffolds can be attributed to the insertion of the f-CNTs between the polymer chains, which facilitated better interactions between the functionalized polymer chains and polar f-CNTs, forming compact

and oriented morphology [45,46]. The average pore diameter was varied with the content of f-CNTs in the polymer matrix. It was 44.25, 91.05, 80.40, and 60.05 μm for CMCS, CMCS/f-CNTs 1, CMCS/f-CNTs 2, and CMCS/f-CNTs 4, respectively. An increase in the pore diameter of the composite hydrogel scaffolds than pure polymer scaffold was assigned to the strong hydrophilic properties of the composite hydrogels due to the presence of the polar groups (–COOH, –OH, $–NH_2$), which facilitated the adsorption of water molecules inside the hydrogels, leading the formation of larger pores [47]. However, the pore size was further decreased with increasing the content of f-CNTs in the polymer matrix. It could be explained by the strong interaction between the functionalized polymer chains and f-CNTs, which caused the minimum availability of the hydrophilic groups to adsorb the water molecules to generate large size-pores. Therefore, less space for the ice crystal formation was available during the freezing process. The smaller ice crystal assisted the formation of a more compact structure with a decrease in the pore size. The highly interconnected and compact structure is favorable for the improved conduction of the charged ions/groups,

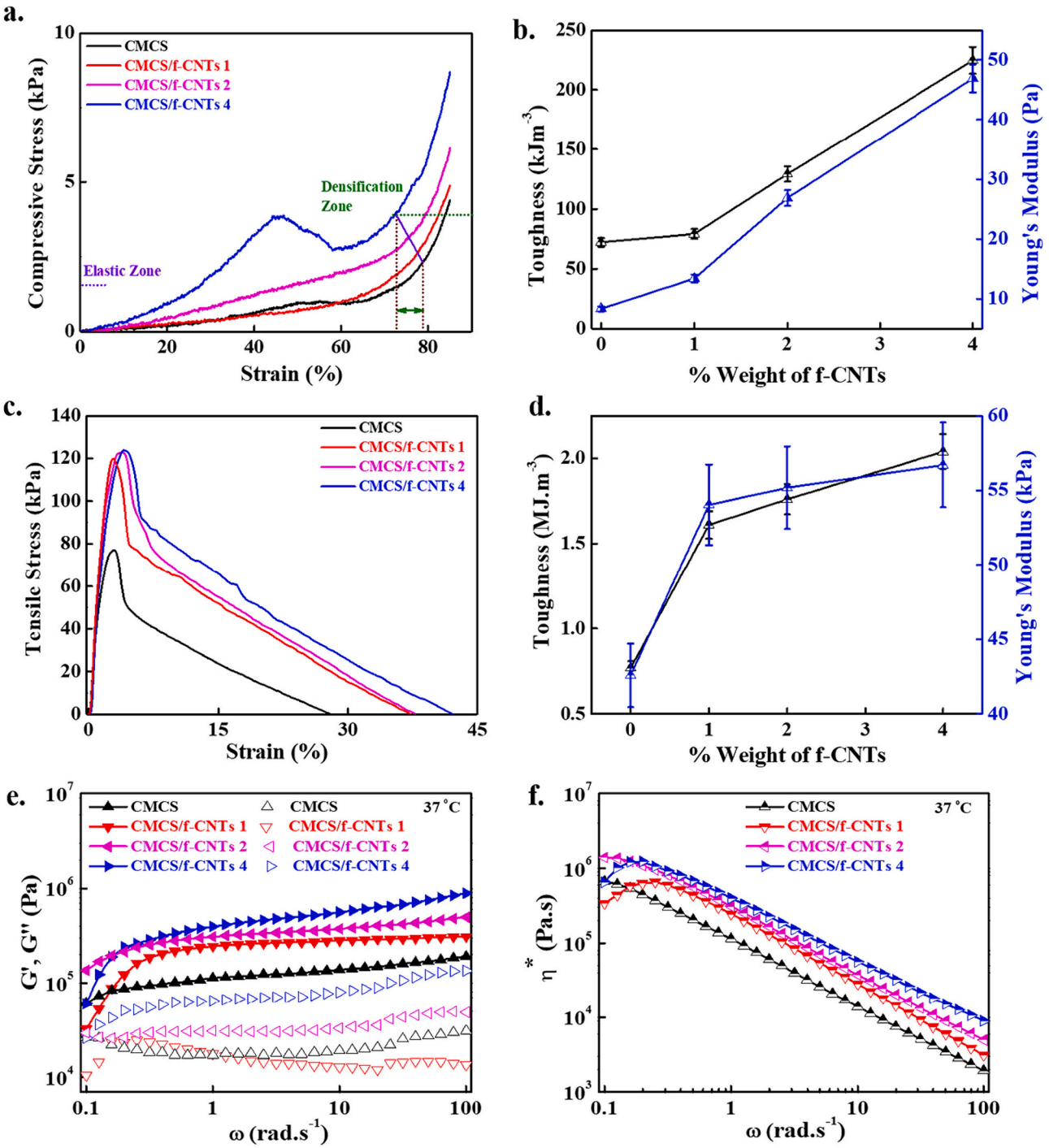

Fig. 2. Assessment of the mechanical strength and viscoelasticity of the developed hydrogels, (a) Stress-strain curves of the indicated hydrogels under compressive mode (speed 10 mm/min), and (b) Toughness and modulus values of the developed hydrogels, (c) Stress-strain curves in elongation mode, (d) Toughness and modulus values of the hydrogel films in elongation mode, (e) Storage and loss moduli of the synthesized hydrogels in the measured angular frequency region of 0.1–100 rad/s at 37 °C, and (f) The corresponding viscosity complex of the developed hydrogels at 37 °C.

which is a desired characteristic for strain sensing applications.

3.2. Mechanical strength and viscoelasticity assessment

The mechanical strength of the developed hydrogels was assessed using the UTM under the compression mode, and the results are shown in (Fig. 2a). The hydrogels show a typical porous scaffold characteristic, including an initial linear region, plateau region, and densification region [48]. An improved compressive strength was observed in the composite hydrogels (8.66 kPa) compared to the pure polymer hydrogel (4.34 kPa) due to the better interactions within hydrogel components [49]. The composite hydrogels demonstrated a lower densification strain than the pure polymer hydrogel, suggesting the more compact structures in the composite hydrogels [50]. The densification strain was 78.82 ± 0.16, 77.60 ± 0.15, 75.52 ± 0.13, and 72.64 ± 0.14 for CMCS, CMCS/f-CNTs 1, CMCS/f-CNTs 2, and CMCS/f-CNTs 4, respectively. The compressive modulus value was obtained by taking the slope of the stress-strain curve at initial linear regions. The toughness value was calculated by considering the area of the strain-strain curves. The compressive modulus and toughness value of the developed hydrogels are given in (Fig. 2b). The compressive modulus values were 8.31, 13.36, 26.83, and 49.92 Pa for CMCS, CMCS/f-CNTs 1, CMCS/f-CNTs 2, and CMCS/f-CNTs 4, respectively. Nearly 6-fold enhancement in the compressive modulus was observed in the composite hydrogels vis-à-vis pure polymer hydrogel. The enhancement in the compressive modulus was assigned to the greater interactions between the functionalized polymer chains and f-CNTs, facilitating the load-transfer process during the measurement [51]. The hydrogels contain abundant active functional groups, including –COOH, –OH, and $–NH_2$ in their matrix. Thus, it is anticipated that the dipole-dipole interaction, hydrogen bonding, and electrostatic interactions play significant roles in enhancing the mechanical strength of the composite hydrogels. An enhancement in the toughness value was also observed in the composite hydrogels, compared to the pure polymer hydrogels, owing to the suppression of the crack propagation process by the added f-CNTs.

The tensile strength of the hydrogel films under dry conditions was also monitored using the UTM, and the obtained stress-strain curves are presented in (Fig. 2c). The f-CNTs assisted hydrogels demonstrated enhanced tensile strength (77.30 → 123.97 kPa) and elongation at the breaks (28 → 42 %) vis-à-vis pure polymer films, showing positive effects of the added nanomaterial on the mechanical strength. The improved mechanical strength of the composite hydrogel films can be attributed to the greater interactions between the polar groups of the f-CNTs and polymer chains, facilitating the effective stress-transfer and enhanced mechanical strength [52]. Spinks and coworkers also reported the enhanced mechanical strength of the chitosan/CNTs microfibers under dry conditions compared to the swelled due to the greater entanglement of the polymer chains, causing the resistance to deformation [53]. The Young's modulus and toughness values of the hydrogel films are given in (Fig. 2d). The Young's modulus was 42.59 ± 1.46, 54.03 ± 1.6, 55.18 ± 1.96, and 56.70 ± 4.56 kPa for CMCS, CMCS/f-CNTs 1, CMCS/f-CNTs 2, and CMCS/f-CNTs 4, respectively. The toughness value was 0.77 ± 0.0014, 1.61 ± 0.012, 1.76 ± 0.008, and 2.04 ± 0.009 $MJ.m^{-3}$ for CMCS, CMCS/f-CNTs 1, CMCS/f-CNTs 2, and CMCS/f-CNTs 4, respectively. The enhanced modulus and toughness values of the composite hydrogel films was attributed to the effective stress transfer and inhibition of the crack propagation process by f-CNTs during the measurement, causing improved mechanical strength. Sun and coworkers also reported enhanced mechanical strength in CNTs-added chitosan nanocomposite films through better interfacial interactions among the added materials [54].

The viscoelastic properties of the developed hydrogels were monitored by a rheometer in the measured regions of 0.1–100 rad/s at 37 °C (body temperature), and the results are presented in (Fig. 2e). No crossover point was observed in all hydrogels, suggesting the solid-like properties. [55]. Interestingly, the composite hydrogels show greater storage modulus (G′, solid line) than the pure polymer hydrogels throughout the measured regions. The storage modulus was further increased with increasing f-CNT contents in the polymer matrix due to the greater interactions between the functionalized polymer chains and f-CNTs, as observed in FTIR results. It is anticipated that hydrogen bonding, dipole-dipole, and electrostatic interactions play crucial roles in the enhancement of the storage modulus of the composite hydrogels [56]. Lin and coworkers developed temperature-sensitive hydrogels using carboxylated chitosan and functionalized carbon nanotubes for drug delivery. They noticed a minor enhancement in the storage modulus in the composite hydrogels to the pure polymer hydrogels [47]. However, in the developed hydrogels, approximately 4.6 folds enhancement in the storage modulus was observed in the composite hydrogels ($1.9 \times 10^5 \rightarrow 8.8 \times 10^5$ Pa) compared to the pure polymer hydrogel at a higher measured region (100 rad/s), indicating improved elasticity due to the greater interactions. This improvement in the storage modulus of the composite hydrogels could be attributed to the relaxation and simultaneous re-constructions of interconnected networks through different interactions, restricting the motion of the polymer chains and leading to the generation of solid-like characteristics and enhanced storage modulus [57]. The loss modulus (G″, without lines) of the developed hydrogels is measured, and the results are also shown in (Fig. 2e). The composite hydrogels demonstrated a higher loss modulus than the pure polymer. However, their values were lower than the respective storage modulus, indicating the elastic characteristics in the hydrogels.

The corresponding complex viscosity (η*) of the developed hydrogels was also monitored in the measured regions of 0.1–100 rad/s at 37 °C. The change in the complex viscosity is given in (Fig. 2f). The composite hydrogels show improved complex viscosity vis-à-vis pure polymer hydrogels and increased with increasing f-CNTs content in the polymer matrix. This enhancement in the complex viscosity can be attributed to the greater interactions between hydrogel components, causing compact structure [58]. The developed hydrogels exhibit an increased complex viscosity at the lower angular frequency regions, followed by a gradual decrease in the complex viscosity, showing the shear thickening and shear thinning characteristics of the hydrogels. The shear thinning and thickening properties assist in good shape fidelity and high accuracy during 3D printing. At a lower angular frequency, interactions between hydrogel components facilitated the randomly oriented functionalized polymer chains in an aligned fashion. They formed a compact structure, leading to improved high complex viscosity. The high deformation force at the higher angular frequency regions caused the disentanglement of the polymer chains. It minimized the interactions among the hydrogel components, decreasing the viscosity complex and generating shear thinning behavior [36].

3.3. 3D-printing of hydrogels

To verify the shear thinning and thickening characteristics of the developed hydrogels, we 3D-printed the constructs using the bioprinter, and the image of the hydrogel during printing is shown in (Fig. 3a). The hydrogels were easily extruded from the needle and formed the pre-designed constructs. The 3D-printed structures of the developed hydrogels are presented in (Fig. 3b). The 3D-printed constructs retained their pre-designed morphology, demonstrating the desirable printing characteristics of the hydrogels. Several factors, such as the viscoelasticity of the hydrogels, printing rate, pressure, and temperature, significantly influence the printing process [59]. A movie file for hydrogel printing is given in the (SI Video 1). The hydrogels were smoothly extruded from the nozzle and adhered to the printed surface. It is necessary that the shear thickening should occur at an appropriate rate to provide sufficient adhesiveness between the printed layers. The inappropriate thickening rate damages the printed morphology. The printability potential of the developed hydrogels was assessed in terms of uniformity factor (U), and the results are presented in (Fig. 3c). This

was 1.0013 ± 0.051, 1.003 ± 0.05, 1.002 ± 0.05, and 0.996 ± 0.049 for CMCS, CMCS/f-CNTs 1, CMCS/f-CNTs 2, and CMCS/f-CNTs 4, respectively. This value is nearly 1, demonstrating the developed hydrogels' uniform printing strand. The composite hydrogels exhibit a decreased uniformity factor vis-à-vis pure polymer hydrogel, suggesting improved printing potential. The improved printing potential of the composite hydrogels can be attributed to the greater interactions between the functionalized polymer chains and f-CNTs, which facilitated shear thickening characteristics at the required rate. The hydrogels with poor viscosity and thixotropic characteristics exhibited non-uniform printing strands [60]. Other factors, including gravity, adhesiveness, temperature, printing rate, and ink characteristics, also influence the uniformity of the printing strands.

The printability characteristic of the developed hydrogels was examined by measuring the expansion ratio (α) of the printed hydrogels. The results are shown in (Fig. 3d). It was 2.24 ± 0.085, 2.01 ± 0.096, 1.93 ± 0.10, and 1.70 ± 0.11 for CMCS, CMCS/f-CNTs 1, CMCS/f-CNTs 2, and CMCS/f-CNTs 4, respectively. The composite hydrogels show a decreased expansion ratio than the pure polymer hydrogels, indicating lesser expansion of the printed strands and improved printability. The decreased expansion ratio of the composite hydrogels can be assigned to the improved viscosity and adhesiveness due to the greater interactions between the functionalized polymer chains and f-CNTs. The adhesiveness characteristic of the developed hydrogels is discussed later in the manuscript. The pore factor (Pr) of the printed hydrogels was also assessed to validate the printability of the developed hydrogels, and the results are presented in (Fig. 3e). It was 1.065 ± 0.053, 1.025 ± 0.051, 1.018 ± 0.05, and 1.01 ± 0.05 for CMCS, CMCS/f-CNTs 1, CMCS/f-CNTs 2, and CMCS/f-CNTs 4, respectively. The composite hydrogels show close to 1 value, suggesting their printing suitability [35]. These findings suggested that the developed hydrogels have superior printing potential and could be explored in developing printed wearable electronic devices for the desired applications.

3.4. Self-healing ability of hydrogel

The self-healing is crucial for wearable electronic devices in strain-sensing applications, where frequent damage occurs through the external or internal factors. The self-healing characteristic enables the additional advantage of restoring the functionality of the devices without using extra materials. The self-healing potential of the developed hydrogels was qualitatively monitored through the cut and healing process at room temperature, and the images are presented in (Fig. 4a). The two halves of the hydrogels were rapidly healed (within 5 m) without using any external factors (temperature, pH, light, *etc.*) showing its self-healing ability. The self-healed hydrogel was easily lifted through the forceps, indicating that the two halves were properly healed. The quantitative self-healing potential of the developed hydrogels was monitored through a rheometer after 5 min of healing, and the results are given in (Fig. 4b). The initial and self-healed storage modulus of CMCS/f-CNTs 1 hydrogel at 100 rad/s was 3.10 × 10^5, 2.14 × 10^5 Pa, respectively. The self-healed hydrogels regained approximately 70 % of their initial storage modulus value after 30 s of healing, showing the superior healing characteristics of the developed hydrogel. The

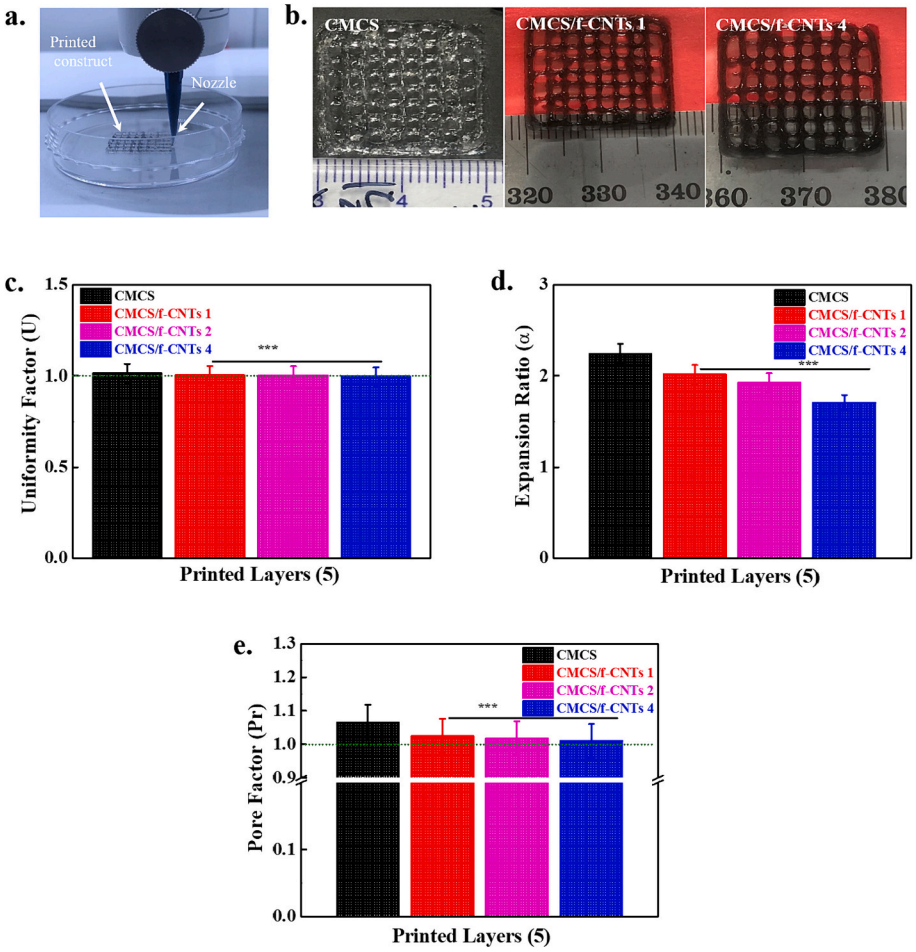

Fig. 3. Assessment of the 3D printing potential of the synthesized hydrogels, (a) Image of the hydrogel during printing, (b) Images of the 3D printed hydrogels, (c) Uniformity factor of the printed hydrogels, (d) Expansion ratio of the printed hydrogels, and (e) Pore factors of the printed hydrogels (Statistical analysis was performed between the pure polymer hydrogels and composite hydrogels).

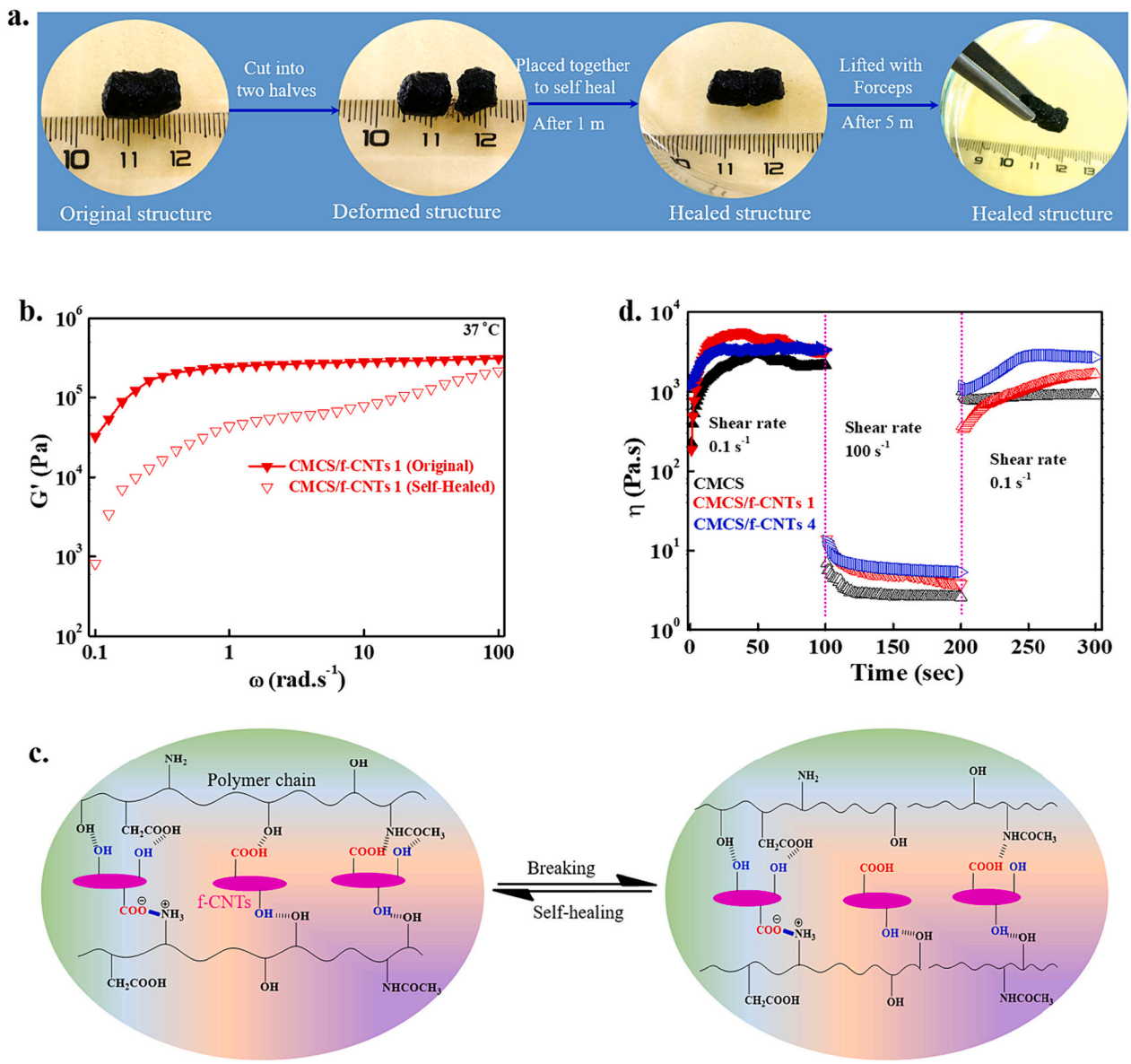

Fig. 4. Monitoring of the self-healing and recovery strength of the synthesized hydrogels, (a) Images of cut and re-joined hydrogels at indicated periods, (b) Change in the storage modulus of self-healed hydrogels vis-à-vis original hydrogel, (c) The plausible self-healing mechanism in the developed hydrogels and (d) Thixotropic behavior of the developed hydrogels at different shear rate at 25 °C.

remarkable self-healing potential of the hydrogel can be attributed to the re-formation of bonds between the hydrogel components through greater interactions [61]. The developed hydrogels have abundant polar groups (–OH, NH_2, $COCH_3$, and COOH), which play significant roles in the regeneration of the bonds. A plausible self-healing mechanism in the developed hydrogels is schematically presented in (Fig. 4c). The bonds were broken during the cutting of the hydrogels and re-formed at the contact through different interactions, such as hydrogen bond, electrostatic interaction, and dipole-dipole interactions. Ren and coworkers also found the rapid self-healing potential in CNTs-added carboxymethyl chitosan-based hydrogels through greater interactions among the added materials [62].

The thixotropic measurement was performed to quantify the recovery and printing characteristics of the developed hydrogels at different shear rates and 37 °C, and the results are shown in (Fig. 4d). The viscosity value was 2146.85, 3225.15, and 3344.21 Pa.s for CMCS, CMCS/f-CNTs 1, and CMCS/f-CNTs 4, at a low shear rate (0.1 s^{-1}), respectively. These values were drastically decreased with increasing the shear rate (100 s^{-1}), and it was 2.5841, 3.7866, and 5.3478 Pa.s for CMCS, CMCS/f-CNTs 1, and CMCS/f-CNTs 4, respectively. This drastic decrease in the viscosity can be attributed to the disruption of the interaction and disentanglement of the functionalized polymer chains within hydrogels [63]. The viscosity value was suddenly increased after removing the high shear rate and reached 895.37, 1638.22, and 2704.96 for CMCS, CMCS/f-CNTs 1, and CMCS/f-CNTs 4, at a low shear rate (0.1 s^{-1}), respectively. These results indicate that the developed hydrogels have remarkable shear thinning and shear thickening characteristics, making them suitable materials for 3D printing applications. The recovery value was 41.58, 50.67, and 80.72 % for CMCS, CMCS/f-CNTs 1, and CMCS/f-CNTs 4, respectively. The composite hydrogels exhibit improved recovery ability vis-à-vis pure polymer hydrogel. The enhanced recovery strength of the composite hydrogels can be attributed to the enhanced interactions (dipole-dipole interaction, hydrogen bonding, and electrostatic) between the functionalized polymer chains and f-CNTs [64]. The recoverable hydrogels have received considerable interest in developing wearable electronic devices. The hydrogels exhibited superior recovery

value, demonstrating their great potential in developing sensing devices for desired applications.

3.5. Adhesiveness of hydrogels

We examined the adhesive properties of the developed hydrogels on different surfaces, including human skin, plastic surfaces, plastic/glass interface, and 3D-printed polymer surfaces, and images are shown in (Fig. 5(i–vi)). The hydrogel was strongly attached to these surfaces, indicating their good adhesive property. We also analyzed the adhesive strength of the hydrogel under load-bearing conditions by filling the 45 mL water in a centrifuge tube, as shown in (Fig. 5(iv)). The developed hydrogels successfully lifted the filled tube, demonstrating its remarkable adhesive strength under load-bearing conditions. The adhesiveness enables additional advantages in developing wearable electronic devices for strain sensing applications due to the lack of requirements of extra adhesive materials like tape or glue, which may cause skin irritations or infections [9]. The quantitative adhesive strength of the developed hydrogels was assessed through the lap shear method on thick paper strips and schematic presentation for the measuring of the adhesive strength is shown in (Fig. 5b). The load-displacement curves of the developed hydrogels were measured using the UTM and the results are presented in (Fig. 5c). An enhanced load-bearing capacity was observed in the composite hydrogels than the pure polymer hydrogels, showing their superior adhesive strength. The enhanced load-bearing capacity of the composite hydrogels can be attributed to the improved interactions between the different functional groups (–COOH, –OH, and $–NH_2$) of the hydrogel components and applied surfaces, facilitating the load transfer process [65]. The image of the stretched paper strips for the adhesive measurement is given in (Fig. S1). It was observed that the hydrogel was strongly adhered to the applied surface during the stretching. The adhesive strength *vs* displacement curves are shown in (Fig. 5d). The composite hydrogels show improved adhesiveness vis-à-vis pure polymer hydrogels and increased with increasing the content of f-CNTs in the polymer matrices, demonstrating their superior adhesiveness. Various factors, including physicochemical characteristics of hydrogels and applied surfaces, amount of the hydrogel used in the experiment, adhesion time, and surrounding conditions (temperature, humidity) widely influence the adhesive strength of the hydrogels [66]. The quantitative adhesive strength of the developed hydrogels is given in (Fig. 5e). It was 88.77 ± 4.43, 92.0 ± 4.6, 108.08 ± 5.4, and 118.47 ± 5.92 kPa for CMCS, CMCS/f-CNTs 1, CMCS/f-CNTs 2, and CMCS/f-CNTs 4, respectively. The developed hydrogels exhibited superior adhesiveness for sensing applications than the previously reported CNTs-based hydrogels [67]. It is believed that the adhesiveness of the developed hydrogels might be further increased with the surface contacting active functional groups, such as ($–COO^-$ and $–NH_3^+$), due to the increased interactions with active functional groups (–COOH, –OH, and $–NH_2$) of the hydrogels. A plausible mechanism for the interaction between the developed hydrogels and human skin is mentioned in (Fig. 5f). It is anticipated that the hydrogel's functional groups strongly interacted with the charged functional groups of the peptide chains of human skin *via* hydrogen bonding, dipole-dipole, and electrostatic interactions.

3.6. Hydrogels cytotoxicity

The biocompatibility of the developed materials is an essential parameter in developing wearable electronic devices for diverse applications. The developed materials should not express any adverse effects on the applied parts of the living organism [68]. We examined HDF cell viability in the presence of the synthesized hydrogels to monitor their cytotoxicity after 24 h of incubation, and the data are shown in (Fig. 6a). The groups without any treatment were set to be controlled. The hydrogels-treated groups exhibited increased OD values compared to the control group, showing the biocompatibility of the developed hydrogels. Furthermore, the OD value increased with the increased f-CNTs' content in the polymer matrix, demonstrating their superior biocompatibility. The enhanced OD value of the composite hydrogels is

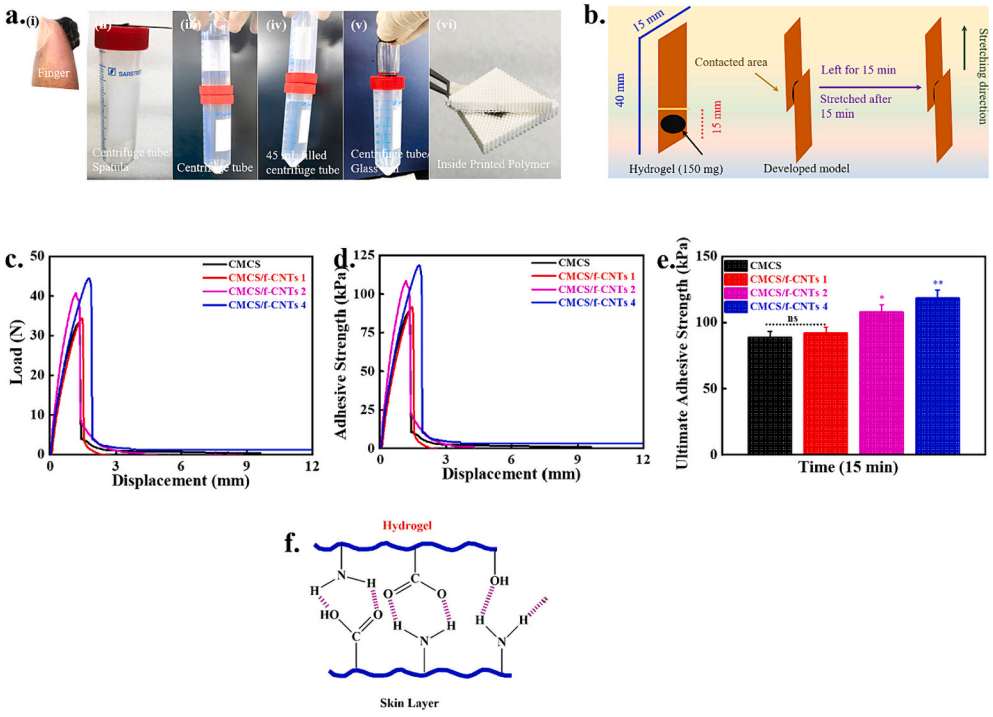

Fig. 5. Examination of the adhesiveness of the prepared hydrogels, (a) Images of adhered hydrogels with different surfaces, including human finger, plastic, glass, and polymer, (b) Schematic presentation for measuring the adhesiveness of the hydrogels, (c) Load *vs.* displacement curves of the synthesized hydrogels, (d) Adhesive strength *vs.* displacement curves of the developed hydrogels, (e) The quantitative values of the adhesive strength, and (f) Possible mechanism for the adhesion of hydrogels to human skin.

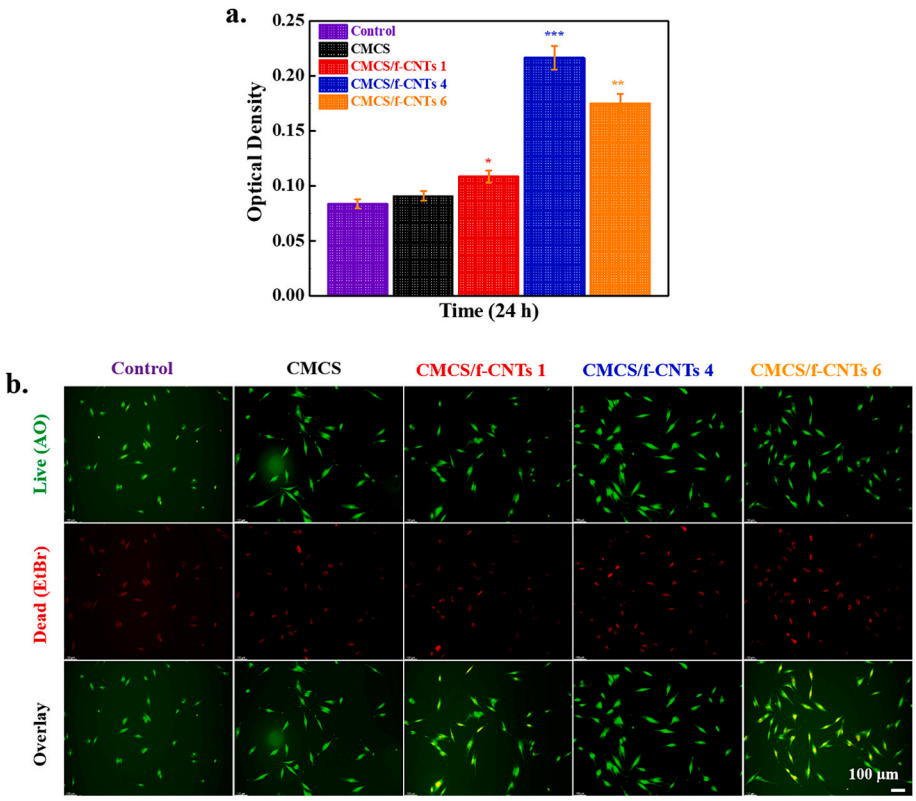

Fig. 6. Assessment of the cytotoxicity of synthesized hydrogels using HDF cells, (a) HDF cell viability with and without hydrogels after 24 h of incubation, and (b) Live/dead assay of HDF cells with and without hydrogels after 24 of incubation.

attributed to the wrapping of the biocompatible polymer chains to f-CNTs and provides more favorable conditions for improved cellular activity [69]. Enhanced cellular activity of the neural cells has been previously reported in the presence of poly(ethylene glycol)/CNTs hydrogels owing to the superior biocompatibility and conductivity [70]. We also examined the biocompatibility of the hydrogels at a higher f-CNTs content (6 wt%) to assess the optimum concentration of f-CNTs for biocompatibility. Interestingly, a decrease in cell viability was observed at a higher f-CNT content in the polymer matrix. The decrease in cell viability can be attributed to the agglomeration of f-CNTs in the polymer matrix, which led to the inappropriate wrapping of the polymer chains, causing toxicity and a decrease in cell viability. The decrease in human vocal fold fibroblast (HVFFs) viability has been earlier reported in glycol chitosan/CNTs-based hydrogels at higher CNT content [71]. We further performed live/dead assay using HDF cells in the presence of the developed hydrogels to validate cell viability results. The images of the live/dead cells after 24 h of incubation are shown in (Fig. 6b). The densities of the live cells were high in hydrogels-treated groups vis-à-vis control, showing the biocompatibility of the prepared hydrogels. This was more significant in f-CNTs-added hydrogels, suggesting that adding f-CNTs has no adverse effect on cellular activity up to 4 wt% of f-CNTs. However, the densities of the dead cells were increased at a higher f-CNTs content (6 wt%). The cell viability results fully supported these findings. Thus, 4 wt% of f-CNTs' contents are ideal for developing biocompatible hydrogels for wearable electronic devices.

3.7. Antibacterial potential

Hydrogels with antibacterial activity have received significant interest in developing wearable electronic devices in the personalized healthcare sector owing to the reduction of microbial contaminations and the increase in the lifespan of the devices [72]. We measured the OD value of the *E. coli* medium with and without hydrogels at different periods (1 and 5 h), and the results are shown in (Fig. 7a). The media without hydrogel treatment were taken as control. A drastic decrease in bacterial growth was observed in the hydrogel-treated groups vis-à-vis control, showing the antibacterial activity of the hydrogels. The antibacterial activity of the developed hydrogels is assigned to the electrostatic interactions of the positively charged polymer chains ($-NH_3^+$) to the negatively charged bacterial cell membrane (phospholipid components), damaging the permeability of the bacterial cell wall and inhibiting the growth of the microorganism [39]. The composite hydrogels exhibited improved antibacterial activity than the pure polymer hydrogel. The enhanced antibacterial activity of the composite hydrogels can be attributed to the wrapping of the charged polymer chains to nanomaterials, leading to greater exposure to the bacterial surface and inhibiting bacterial growth to a greater extent. The enhanced antibacterial activity of the chitosan/CNTs hydrogels has been earlier reported due to the greater electrostatic interactions of the positively charged polymer chains to the bacterial cell membranes [73]. The OD value of the grown bacteria was also measured for extended periods (6 and 24 h) to support the antibacterial characteristics in the developed materials, and the results are shown in (Fig. S2). The composite hydrogels demonstrated a reduced OD value compared to the controls and pure hydrogels, suggesting improved antibacterial potential.

We also examined the bacterial growth through the agar diffusion method to validate the findings above, and the images of the culture plate after 24 h of incubation are shown in (Fig. 7b). The plates without hydrogel treatment were considered as control. The hydrogels-treated groups demonstrated lesser bacteria growth than the control groups, showing antibacterial potential. The composite hydrogels-treated plates exhibited significantly reduced bacteria colonies than the pure polymer and control plates, showing improved antibacterial activity. This finding matches the OD result well. Thus, the developed hydrogels have antibacterial activity and can be explored in the development of wearable electronic devices.

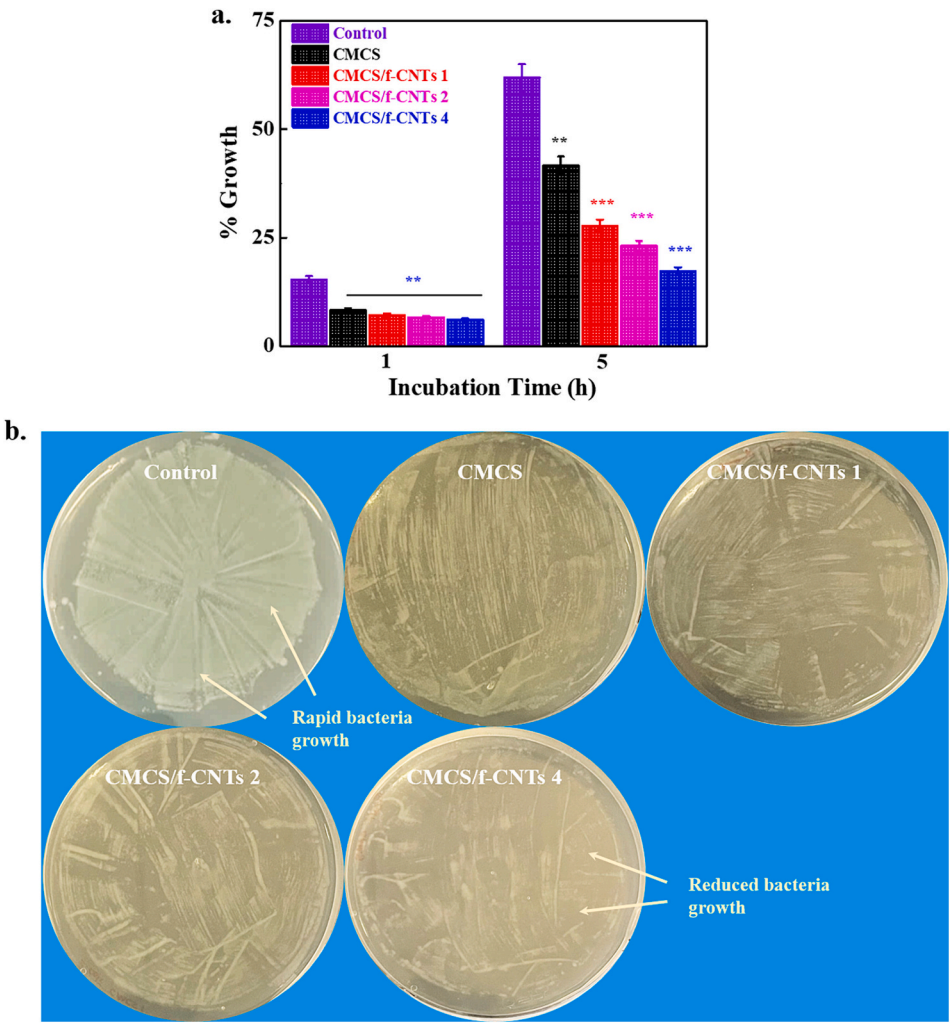

Fig. 7. Examination of the antibacterial potential of the synthesized hydrogels against *E. coli*, (a) OD value of the bacteria media treated with or without hydrogels at indicated periods, (b) Images of growth bacteria on an agar plate with and without hydrogels after 24 h of incubation.

3.8. Electrochemical activity and sensing ability of hydrogels

Electrical conductivity is necessary for developing wearable electronic devices for strain-sensing applications. The conductance property of the developed hydrogels was monitored through the I-V curve at room temperature, and the results are presented in (Fig. 8a). The developed hydrogels exhibited a linear and non-hysteretic curve, demonstrating their electro-conductive characteristics. The conductance values were 0.006, 0.011, and 0.016 mS for CMCS, CMCS/f-CNTs 1, and CMCS/f-CNTs 4 hydrogels, respectively. The improved conductivity of the composite hydrogels can be attributed to the formation of the ion-conductive channels in the hydrogels, which facilitated the migration of the conductive ions at the applied voltage. It is also believed that the prepared f-CNTs have abundant functional groups (–COOH, –OH, and –C–O–C) in their structure, creating the negatively charged surface, forming the conductive channels, and improving conductivity [32]. The composite hydrogels exhibited rough and aligned surface features vis-à-vis pure polymer hydrogels due to the added f-CNTs, as observed in SEM images (Fig. 1e), accelerating the rapid transport of the conductive ions through conductive pathways, which is desirable for strain sensing. The 4 % weight of f-CNTs is considered suitable for strain-sensing measurement due to the cytotoxicity concerns beyond that limits as observed in (Fig. 6a). The hydrogel's conductivity can be further enhanced by inserting the conductive polymers [74,75]. Li and co-workers developed carboxymethyl cellulose-based conductive hydrogels using poly(alinine) as high-performance self-powered strain sensors. The high conductivity was attributed to the formation of effective ionic pathways, which assisted in conduction [76].

We further examined the current change in the hydrogel at different angles (0, 30, 45, and 90°) to monitor the current change in bending and stretching processes, and the results are given in (Fig. 8b). Here, we selected CMCS/f-CNTs 4 hydrogel for further studies owing to its superior electrochemical potential than others hydrogels. The hydrogel exhibits a steady current under straight conditions and significantly decreases with increased finger bending angles (0° → 90°). The decrease in the hydrogel current with increasing the bending angles can be explained by the enhancement of the distance between the conductive groups during the bending process, which restricted the migration of the conductive ions and increased resistance. The distance between the conductive groups was significantly increased at a higher bending angle (90°), leading to a significant enhancement in the resistance and consequently decreased current [77,78]. We further measured the current value by reversing the bending process (90° → 0°) to analyze its recovery potential after removing the strain. The hydrogel regained its initial current value, showing good strain-induced current changeability. This characteristic is highly desirable in developing wearable electronic devices in the personalized healthcare sector. Moreover, we monitored the current change value in the hydrogel in three successive steps of the cutting and self-healing process to analyze the self-healing efficiency and its effects on hydrogel conductivity. The current change

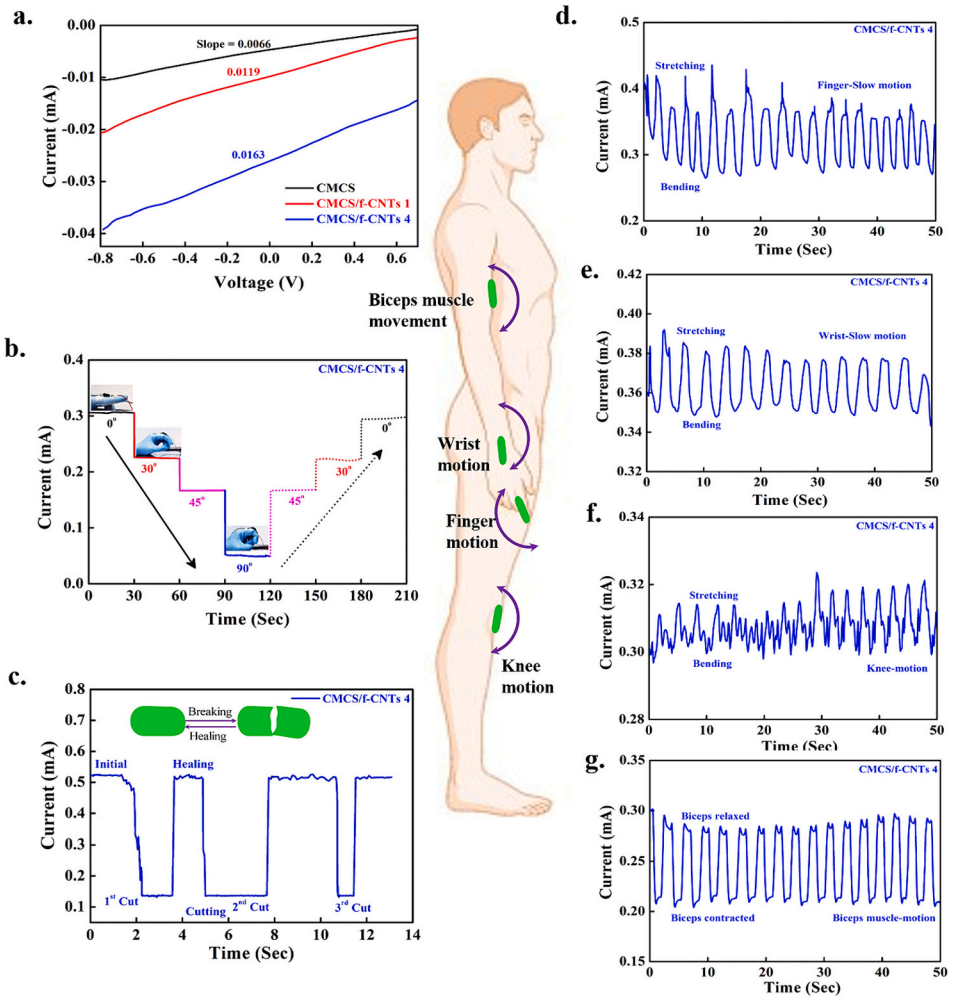

Fig. 8. Examination of the strain-sensing potential of the developed hydrogels, (a) I—V curves of the indicated hydrogels, (b) Change in the hydrogel current at different angles, (c) Change in the hydrogel current during cutting and healing process, (d) The generated waveforms during slow motion of human finger, (e) During slow motion of wrist, (f) rapid motion of knee, and (g) Recognition of the biceps motion.

in the hydrogels after self-healing is given in (Fig. 8c). Initially, hydrogel shows a steady current value (0.5227 mA), which drastically dropped in cutting conditions due to the disruption of the conductive pathways. The hydrogel nearly recovered its initial current value (0.5201 mA) after self-healing due to the rebuilding of the effective conductive channels, showing the remarkable self-healing potential of the hydrogel. A similar current value was observed throughout the process, demonstrating the superior self-healing characteristic. The conductive and self-healing hydrogels have received considerable interest in fabricating wearable electronic devices for different applications due to the increased durability of the fabricated devices [79]. Before performing the strain-sensing potential of the hydrogel, we checked its adhesiveness on the surface of the finger under normal and inverted conditions. The images are given in (Fig. S3). The hydrogel was adequately attached to the surface of the finger in both conditions, which is desirable for strain-sensing applications.

The real-time strain-sensing potential of the hydrogel was examined at the different human body parts, including finger, wrist, elbow, and knee. We have selected CMCS/f-CNTs 4 hydrogel to assess the strain-sensing potential owing to its superior electrochemical performance to other hydrogels. The stretching and bending processes were performed to measure the strain-sensing ability of the hydrogel. The generated waveforms under the slow motion of the human finger are shown in (Fig. 8d). The hydrogel exhibits nearly uniform waveforms during the stretching and bending of the finger, indicating the real-time motion-sensing potential of the hydrogel. A decrease in the current value occurred during the bending condition of the motion due to the enhancement of the distance between the conductive pathways, which hindered the flow of the conductive groups and caused a decrease in current. The magnitude of the finger bending and stretching process profoundly influences the patterns of the formed waveforms. We also measured the finger motion sensing potential of the hydrogels under speedy conditions, and the generated waveforms are presented in (Fig. S4). A steady waveform was generated during the stretching and bending process of the finger, indicating its strain-sensing ability. However, the densities of the generated waveforms were high compared to the slow motion of the finger due to the rapid change in the current flow during motions. We further assessed the motion-sensing ability of the developed hydrogel at the wrist, elbow, and knee parts of the human body, and the generated waveforms are given in (Fig. 8(e–f)). The hydrogel exhibits nearly similar waveforms during the motion of the different human body parts, demonstrating its good strain-sensing ability and fidelity for motion-sensing applications. We also performed the wrist motion sensing potential of the hydrogels under speedy conditions, and the generated waveforms are presented in (Fig. S5). A greater and nearly uniform waveform was generated during the rapid stretching and bending process of the wrist, showing its superior strain-sensing ability. We also monitored the strain-sensing ability of the developed hydrogels for different cycles to validate the repeatability potential at the human finger. The generated waveforms are given

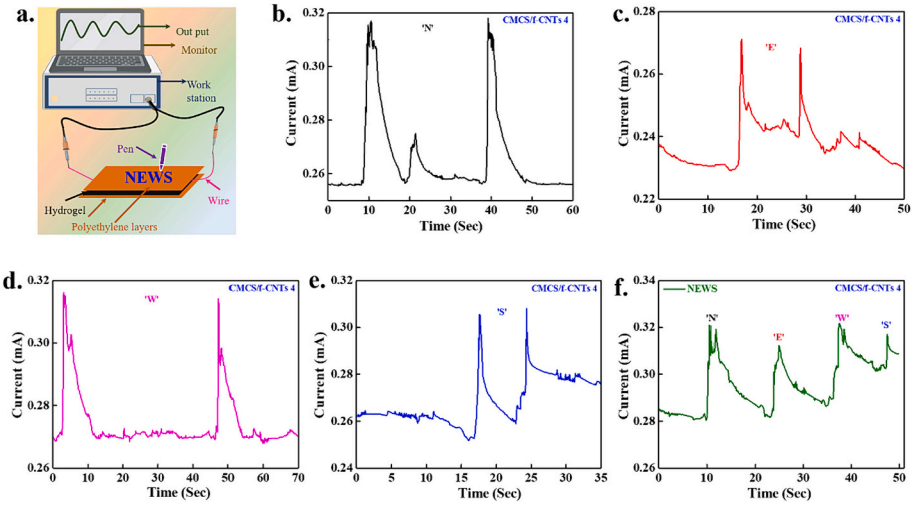

Fig. 9. Monitoring of the multidimensional motion recognition ability of the developed hydrogels, (a) Schematic presentation for the designed device, (b–e) The corresponding generated waveforms of different letters, and (f) The combined generated waveforms of the "NEWS" letter during writing on hydrogel surface.

(Fig. S6). Nearly uniform waveforms were generated in all cycles of finger motion, showing the superior repeatability potential of the hydrogels. These results indicated that the prepared hydrogel has the potential to develop wearable electronic devices for strain-sensing applications.

We further explored the muscle contraction and relaxation sensing potential of the developed hydrogel, and the generated waveforms are shown in (Fig. 8g). Nearly uniform waveforms were generated during the contraction and relaxation of the muscle, demonstrating the hydrogel real-time sensing potential for minor biceps movement. The current value decreased during the muscle contraction owing to its swelling, which generated the strain in the hydrogel with increased resistance and consequently decreased the current value. The generated patterns significantly depend on muscle contraction and relaxation process magnitude. We measured resistance changes in the hydrogels at different strains, and the curve of relative resistance change *vs* the applied strain from 0 to 210 % is presented in (Fig. S7a). Nearly linear change in the relative resistance was observed with applied strain, demonstrating the hydrogel has wide strain working potential and superior strain responsiveness [80]. The strain sensitivity of the hydrogel was determined in terms of gauge factor (GF), and the curve of GF *vs.* applied strain is shown in (Fig. S7b). The GF was 2.4 at 210 % strain, showing the superior strain sensitivity of the hydrogel. The hydrogels immediately exhibited the sensing potential after applying the strain. This value is higher than the previously reported chitosan-based conductive hydrogels, indicating the enhanced strain sensitivity of the hydrogels [21]. Most of the developed electronic devices can only detect one-dimensional activity, such as the motion of the body parts, and fail to recognize multidimensional movement. Hydrogels with multidimensional movement recognition abilities have received considerable interest in developing wearable electronic devices for diverse applications [81]. Auditory or speech-impaired persons extensively use sign language in communicating information. To explore the multidimensional movement recognition potential of the developed hydrogels, we sandwiched the hydrogel between two thin polyethylene films. We connected it with the wires connected to the source meter. The schematic presentation for the developed device is given in (Fig. 9a). A pen was used to write different English letters, including "N", "E", "W", and "S", as well as the word "NEWS" on the surface of the developed device. The generated waveforms are shown in (Fig. 9(b–e)). An individual letter was written twice to monitor the repeatability behavior of the developed hydrogel. Different letters generated specific waveforms, and similar waveforms were observed when the letter was repeated, indicating the superior repeatability and sensitivity of the developed hydrogel. The magnitude of the generated waveforms varies from letter to letter and highly depends upon the letter writing speed, applied pressure/force, and motion tracking [82]. Furthermore, when the individual letter was written in the word form "NEWS", and the generated waveforms are presented in (Fig. 9f). The generated waveforms were nearly identical to their initial patterns, as observed in (Fig. 9(b–e)). These results indicate the multidimensional movement recognition ability of the developed hydrogel and can be explored in developing wearable electronic devices for desired applications. A comparative examination of the advantages and disadvantages of the previously published works with current work is also summarized in Table 1 [62,83–87]. The hydrogels demonstrated good printability characteristics with strain-sensing potential.

4. Conclusion

The multifunctional 3-printable hydrogels of carboxymethyl chitosan and f-CNTs were developed *via* a one-pot strategy for strain-sensing applications. The developed hydrogels were characterized through different spectroscopic techniques, including FTIR and XRD analysis. The pure polymer (CMCS) hydrogel scaffold exhibited a randomly oriented morphology, whereas an aligned structure was observed in the composite hydrogel scaffolds. The composite hydrogels showed improved mechanical and viscoelastic characteristics vis-à-vis pure polymer hydrogels due to the greater interactions between the polar groups of the functionalized polymer and f-CNTs. The developed hydrogels exhibited superior adhesive strength, and this potential was increased with increased content of the f-CNTs in the polymer matrix. The developed hydrogels showed rapid self-healing ability, and the two halves were rapidly healed (within 5 min) without applying any external factors, such as temperature, pH, light, *etc.* The hydrogels also demonstrated remarkably enhanced thixotropic characteristics with an 80.72 % recovery value.

The biocompatibility of the hydrogels was monitored using human dermal fibroblast cells through WST-8 assay. The developed hydrogels have no adverse effects on cultured cells, indicating their biocompatibility. The developed hydrogels also showed antibacterial potential against *Escherichia coli*. The composite hydrogels demonstrated superior electrochemical properties than the pure polymer hydrogel due to the effective transport of the conductive groups through the conductive pathways. The motion-sensing ability of the hydrogel was examined at different parts of the human body, such as finger, wrist, elbow, and knee. The developed hydrogel showed a uniform waveform during the motion of the body parts, suggesting its motion-sensing ability. The hydrogel

Table 1
The comparative analysis of the advantages and disadvantages of previously reported chitosan-based hydrogels with current work for strain sensing.

Hydrogel component	Advantages	Limitations	References
Carboxymethyl chitosan/ Poly(acrylamide) /CNTs	Excellent mechanical strength (tensile strength of 475.4 kPa, and compressive strength of 1.9 MPa) Superior conductivity (0.19 S. cm^{-1}) Real-time human body motion and writing signals potential	Low gauge factor (1.154 at 200 % strain)	[83]
Carboxymethyl chitosan/ Poly(acrylamide) /Poly(aniline)	Excellent stretchability (~1100 %) Enhanced conductivity (0.45 mS. cm^{-1}) Antibacterial Biocompatible Good strain sensitivity (GF = 6.43)	Moderate adhesiveness (~22.6 kPa)	[84]
Chitosan/ Poly(pyrrole)	Good mechanical strength (251.48 kPa at the fracture strain of 2149.17 %) Improved adhesive strength (~51.54 kPa) Enhanced conductivity (0.534 S. m^{-1}) Biocompatible Real-time motion sensing with excellent stability (1000 times)	Moderate gauge factor (1.88 at 200 % strain)	[85]
Carboxymethyl chitosan/ Poly(vinyl alcohol) /CNTs	Rapid self-healing (97 % within 15 s) Enhanced mechanical strength (0.186 MPa) Excellent stretchability (2600 %) Antibacterial Biocompatible Real-time motion sensing of porcine lungs and rat heart beatings	Gauge factor not examined	[62]
Carboxymethyl chitosan/ Poly(acrylamide) /Sodium chloride	Enhanced mechanical strength (430 kPa, at 1100 % strain) Excellent conductivity (6.44 S. m^{-1}) Anti-freezing property Good water retention potential Real-time human motion sensing	Low gauge factor (0.214 at 0.5–300 % strain)	[86]
Chitosan/ Poly(acrylamide) /Al^{3+}	High transparency (>90 % at 800 nm) Superior electrical conductivity (5.01 S. m^{-1}) Enhanced mechanical strength (730 kJ/m^3 toughness) Self-healing Human motion sensing Pressure sensing	Moderate gauge factor (3.0 at 100–600 % strain)	[87]
Carboxymethyl chitosan/ Unzipped CNTs	3D printable Enhanced viscoelasticity (Storage modulus: 8.8×10^5 Pa) Rapid self-healing Excellent recovery potential (80.72 %) Superior adhesiveness (118 ± 5.92 kPa) Real-time human motion sensing Complex letter recognition ability Good gauge factor (2.4 at 210 % strain)	–	In this study

also detected the motion of the muscles. Furthermore, the developed hydrogel was explored in letter sensing to monitor the multidimensional movement recognition ability. The developed hydrogel precisely demonstrates multidimensional movement recognition capability and has the potential to fabricate wearable electronic devices for strain-sensing applications. However, more detailed studies under normal and harsh conditions are required to demonstrate the strain-sensing potential of the developed hydrogels for practical applications.

Supplementary data to this article can be found online at https://doi.org/10.1016/j.ijbiomac.2024.131025.

CRediT authorship contribution statement

Dinesh K. Patel: Writing – original draft, Formal analysis, Data curation, Conceptualization. **So-Yeon Won:** Formal analysis. **Tejal V. Patil:** Data curation. **Sayan Deb Dutta:** Data curation. **Ki-Taek Lim:** Visualization. **Sung Soo Han:** Project administration.

Declaration of competing interest

The authors declare that they have no known competing financial interests or personal relationships that could have appeared to influence the work reported in this paper.

Data availability

Data will be made available on request.

Acknowledgments

This work is supported by the Korea Institute of Planning and Evaluation for Technology in Food, Agriculture and Forestry (IPET) through High Value-added Food Technology Development Program, funded by Ministry of Agriculture, Food and Rural Affairs (MAFRA) (321027-5). This research is supported by the National Research Foundation of Korea (NRF) (2020R1A6A1A03044512). This work is also supported by Ministry of Education of Korea (NRF Grant Numbers: 2018R1A16A1A03025582 and 2022R1I1A3063302).

Human or animal rights

The experiment was performed with the help of the first author as volunteer (Age: 36, Sex: Male, and Ethnicity: Asian) and obtained informed consent to publish images and data. This study met the guidelines in authors' guidelines.

References

[1] Z. Chen, Y. Chen, M.S. Hedenqvist, C. Chen, C. Cai, H. Li, H. Liu, J. Fu, Multifunctional conductive hydrogels and their applications as smart wearable devices, J. Mater. Chem. B 9 (11) (2021) 2561–2583.
[2] X. Wang, Z. Bai, M. Zheng, O. Yue, M. Hou, B. Cui, R. Su, C. Wei, X. Liu, Engineered gelatin-based conductive hydrogels for flexible wearable electronic devices: fundamentals and recent advances, J. Sci. Adv. Mater. Devices 7 (3) (2022).
[3] G. Yang, J. Ding, B. Yang, X. Wang, C. Gu, D. Guan, Y. Yu, Y.-M. Zhang, S.X.-A. Zhang, Highly stretchable electrochromic hydrogels for use in wearable electronic devices, J. Mater. Chem. C 7 (31) (2019) 9481–9486.

[4] Y.G. Park, G.Y. Lee, J. Jang, S.M. Yun, E. Kim, J.U. Park, Liquid metal-based soft electronics for wearable healthcare, Adv. Healthc. Mater. 10 (17) (2021).
[5] C.A. Silva, J. Lv, L. Yin, I. Jeerapan, G. Innocenzi, F. Soto, Y.G. Ha, J. Wang, Liquid metal based island-bridge architectures for all printed stretchable electrochemical devices, Adv. Funct. Mater. 30 (30) (2020).
[6] H. Zhou, Z. Wang, W. Zhao, X. Tong, X. Jin, X. Zhang, Y. Yu, H. Liu, Y. Ma, S. Li, W. Chen, Robust and sensitive pressure/strain sensors from solution processable composite hydrogels enhanced by hollow-structured conducting polymers, Chem. Eng. J. 403 (2021).
[7] Z. Shen, Z. Zhang, N. Zhang, J. Li, P. Zhou, F. Hu, Y. Rong, B. Lu, G. Gu, High-stretchability, ultralow-hysteresis conducting polymer hydrogel strain sensors for soft machines, Adv. Mater. 34 (32) (2022).
[8] J. Song, C. Mou, G. Balakrishnan, Y. Wang, M. Rajagopalan, A. Schreiner, D. Naik, T. Cohen-Karni, M.S. Halbreiner, C.J. Bettinger, Hysteresis-free and high-sensitivity strain sensing of ionically conductive hydrogels, Adv. NanoBiomed Res. 3 (2) (2022).
[9] S.D. Sahoo, T.K. Vasudha, V. Muthuvijayan, E. Prasad, Chitosan-based self-healable and adhesive hydrogels for flexible strain sensor application, ACS Appl. Polym. Mater. 4 (12) (2022) 9176–9185.
[10] Q. Zhang, X. Liu, L. Duan, G. Gao, Ultra-stretchable wearable strain sensors based on skin-inspired adhesive, tough and conductive hydrogels, Chem. Eng. J. 365 (2019) 10–19.
[11] H. Cheng, W. Zhang, R. Pan, J. Yang, Y. Gong, Y. Zhuo, F. Wang, X. Yuan, Z. Gan, R. Hu, J. Ding, L. Chen, X. Zhang, X. Tian, Poly(vinyl alcohol), tannic acid, and silver-based hydrogel strain sensors with "fish scale-like" surfaces, ACS Appl. Polym. Mater. 5 (6) (2023) 4146–4158.
[12] C. Zhang, Y. Zhou, H. Han, H. Zheng, W. Xu, Z. Wang, Dopamine-triggered hydrogels with high transparency, self-adhesion, and thermoresponse as skinlike sensors, ACS Nano 15 (1) (2021) 1785–1794.
[13] X. Qu, S. Wang, Y. Zhao, H. Huang, Q. Wang, J. Shao, W. Wang, X. Dong, Skin-inspired highly stretchable, tough and adhesive hydrogels for tissue-attached sensor, Chem. Eng. J. 425 (2021).
[14] X. Zhang, S. Lin, L. Zhang, R. Guo, Y. Lu, S. Liu, Z. Su, Z. Ji, X. Wang, 3D printable conductive ionic hydrogels with self-adhesion performance for strain sensing, J. Mater. Chem. C 10 (38) (2022) 14288–14295.
[15] A.N. Raja, Recent development in chitosan-based electrochemical sensors and its sensing application, Int. J. Biol. Macromol. 164 (2020) 4231–4244.
[16] Y. Fang, J. Xu, F. Gao, X. Du, Z. Du, X. Cheng, H. Wang, Self-healable and recyclable polyurethane-polyaniline hydrogel toward flexible strain sensor, Compos. Part B Eng. 219 (2021).
[17] D.K. Patel, K. Ganguly, S.D. Dutta, T.V. Patil, K.-T. Lim, Multifunctional hydrogels of polyvinyl alcohol/polydopamine functionalized with carbon nanomaterials as flexible sensors, Mater. Today Commun. 32 (2022).
[18] L. Xu, X. Liang, L. You, Y. Yang, G. Fen, Y. Gao, X. Cui, Temperature-sensitive poly (N-isopropylacrylamide)-chitosan hydrogel for fluorescence sensors in living cells and its antibacterial application, Int. J. Biol. Macromol. 189 (2021) 316–323.
[19] S. Wu, C. Xu, Y. Zhao, W. Shi, H. Li, J. Cai, F. Ding, P. Qu, Recent advances in chitosan-based hydrogels for flexible wearable sensors, Chemosensors 11 (1) (2023).
[20] S. Liu, Z. Liu, M. Wu, X. Xu, F. Huang, L. Zhang, Y. Liu, Q. Shuai, NIR as a "trigger switch" for rapid phase change, on-demand release, and photothermal synergistic antibacterial treatment with chitosan-based temperature-sensitive hydrogel, Int. J. Biol. Macromol. 191 (2021) 344–358.
[21] Y. Yang, M. Zhou, J. Peng, X. Wang, Y. Liu, W. Wang, D. Wu, Robust, anti-freezing and conductive bonding of chitosan-based double-network hydrogels for stable-performance flexible electronic, Carbohydr. Polym. 276 (2022).
[22] K. Yan, Y. Wan, F. Xu, J. Lu, C. Yang, X. Li, Z. Lu, X. Wang, D. Wang, Ionic crosslinking of alginate/carboxymethyl chitosan fluorescent hydrogel for bacterial detection and sterilization, Carbohydr. Polym. 302 (2023).
[23] X. Sun, Z. Qin, L. Ye, H. Zhang, Q. Yu, X. Wu, J. Li, F. Yao, Carbon nanotubes reinforced hydrogel as flexible strain sensor with high stretchability and mechanically toughness, Chem. Eng. J. 382 (2020).
[24] B. Wang, L. Dai, L.A. Hunter, L. Zhang, G. Yang, J. Chen, X. Zhang, Z. He, Y. Ni, A multifunctional nanocellulose-based hydrogel for strain sensing and self-powering applications, Carbohydr. Polym. 268 (2021).
[25] R. Zhao, L. Jiang, P. Zhang, D. Li, Z. Guo, L. Hu, Graphene oxide-based composite organohydrogels with high strength and low temperature resistance for strain sensors, Soft Matter 18 (6) (2022) 1201–1208.
[26] K. Feng, G.-Y. Hung, X. Yang, M. Liu, High-strength and physical cross-linked nanocomposite hydrogel with clay nanotubes for strain sensor and dye adsorption application, Compos. Sci. Technol. 181 (2019).
[27] R. Fang, K. Chen, L. Yin, Z. Sun, F. Li, H.-M. Cheng, The regulating role of carbon nanotubes and graphene in lithium-ion and lithium-sulfur batteries, Adv. Mater. 31 (9) (2019).
[28] M. Qu, H. Wang, Q. Chen, L. Wu, P. Tang, M. Fan, Y. Guo, H. Fan, Y. Bin, A thermally-electrically double-responsive polycaprolactone – thermoplastic polyurethane/multi-walled carbon nanotube fiber assisted with highly effective shape memory and strain sensing performance, Chem. Eng. J. 427 (2022).
[29] P. Ahuja, S.K. Ujjain, K. Urita, A. Furuse, I. Moriguchi, K. Kaneko, Chemically and mechanically robust SWCNT based strain sensor with monotonous piezoresistive response for infrastructure monitoring, Chem. Eng. J. 388 (2020).
[30] G. Georgousis, C. Pandis, A. Kalamiotis, P. Georgiopoulos, A. Kyritsis, E. Kontou, P. Pissis, M. Micusik, K. Czanikova, J. Kulicek, M. Omastova, Strain sensing in polymer/carbon nanotube composites by electrical resistance measurement, Compos. Part B Eng. 68 (2015) 162–169.
[31] Z. Qin, X. Sun, Q. Yu, H. Zhang, X. Wu, M. Yao, W. Liu, F. Yao, J. Li, Carbon nanotubes/hydrophobically associated hydrogels as ultrastretchable, highly sensitive, stable strain, and pressure sensors, ACS Appl. Mater. Interfaces 12 (4) (2020) 4944–4953.
[32] D.K. Patel, S.D. Dutta, K. Ganguly, J.W. Kim, K.T. Lim, Enhanced osteogenic potential of unzipped carbon nanotubes for tissue engineering, J. Biomed. Mater. Res. A 109 (10) (2021) 1869–1880.
[33] D.K. Patel, K. Ganguly, J. Hexiu, S.D. Dutta, T.V. Patil, K.-T. Lim, Functionalized chitosan/spherical nanocellulose-based hydrogel with superior antibacterial efficiency for wound healing, Carbohydr. Polym. 284 (2022).
[34] L. Zhou, H. Ramezani, M. Sun, M. Xie, J. Nie, S. Lv, J. Cai, J. Fu, Y. He, 3D printing of high-strength chitosan hydrogel scaffolds without any organic solvents, Biomater. Sci. 8 (18) (2020) 5020–5028.
[35] T. Kreller, T. Distler, S. Heid, S. Gerth, R. Detsch, A.R. Boccaccini, Physico-chemical modification of gelatine for the improvement of 3D printability of oxidized alginate-gelatine hydrogels towards cartilage tissue engineering, Mater. Des. 208 (2021).
[36] D.K. Patel, T.V. Patil, K. Ganguly, S.D. Dutta, K.-T. Lim, Nanocellulose-assisted 3D-printable, transparent, bio-adhesive, conductive, and biocompatible hydrogels as sensors and moist electric generators, Carbohydr. Polym. 315 (2023).
[37] D.K. Patel, S.D. Dutta, J. Hexiu, K. Ganguly, K.-T. Lim, Bioactive electrospun nanocomposite scaffolds of poly(lactic acid)/cellulose nanocrystals for bone tissue engineering, Int. J. Biol. Macromol. 162 (2020) 1429–1441.
[38] K. Ganguly, S.D. Dutta, A. Randhawa, D.K. Patel, T.V. Patil, K.T. Lim, Transcriptomic changes toward osteogenic differentiation of mesenchymal stem cells on 3D-printed GelMA/CNC hydrogel under pulsatile pressure environment, Adv. Healthc. Mater. 12 (11) (2023).
[39] D.K. Patel, S.D. Dutta, K. Ganguly, K.-T. Lim, Multifunctional bioactive chitosan/cellulose nanocrystal scaffolds eradicate bacterial growth and sustain drug delivery, Int. J. Biol. Macromol. 170 (2021) 178–188.
[40] M. Fernandes Queiroz, K. Melo, D. Sabry, G. Sassaki, H. Rocha, Does the use of chitosan contribute to oxalate kidney stone formation? Mar. Drugs 13 (1) (2014) 141–158.
[41] B. Doshi, E. Repo, J.P. Heiskanen, J.A. Sirviö, M. Sillanpää, Effectiveness of N,O-carboxymethyl chitosan on destabilization of Marine Diesel, Diesel and Marine-2T oil for oil spill treatment, Carbohydr. Polym. 167 (2017) 326–336.
[42] D. Aztatzi-Pluma, E.O. Castrejón-González, A. Almendarez-Camarillo, J.F. J. Alvarado, Y. Durán-Morales, Study of the molecular interactions between functionalized carbon nanotubes and chitosan, J. Phys. Chem. C 120 (4) (2016) 2371–2378.
[43] I.M. Garnica-Palafox, H.O. Estrella-Monroy, N.A. Vázquez-Torres, M. Álvarez-Camacho, A.E. Castell-Rodríguez, F.M. Sánchez-Arévalo, Influence of multi-walled carbon nanotubes on the physico-chemical and biological responses of chitosan-based hybrid hydrogels, Carbohydr. Polym. 236 (2020).
[44] A.A. Menazea, M.M. Eid, M.K. Ahmed, Synthesis, characterization, and evaluation of antimicrobial activity of novel Chitosan/Tigecycline composite, Int. J. Biol. Macromol. 147 (2020) 194–199.
[45] J. Venkatesan, B. Ryu, P.N. Sudha, S.-K. Kim, Preparation and characterization of chitosan–carbon nanotube scaffolds for bone tissue engineering, Int. J. Biol. Macromol. 50 (2) (2012) 393–402.
[46] L. Suo, H. Wu, P. Wang, Z. Xue, J. Gao, J. Shen, The improvement of periodontal tissue regeneration using a 3D -printed carbon nanotube/chitosan/sodium alginate composite scaffold, J Biomed Mater Res B Appl Biomater 111 (1) (2022) 73–84.
[47] T. Lin, J. Zhang, H. Long, F. Yang, L. Huang, S.-P. Deng, J. Zhang, X. Cai, Y. Yang, S. Tan, Temperature-sensitive hydrogels containing carboxylated chitosan-modified carbon nanotubes for controlled drug release, ACS Appl. Nano Mater. 5 (8) (2022) 10409–10420.
[48] R. Olmos-Juste, B. Alonso-Lerma, R. Pérez-Jiménez, N. Gabilondo, A. Eceiza, 3D printed alginate-cellulose nanofibers based patches for local curcumin administration, Carbohydr. Polym. 264 (2021).
[49] G. Li, C. Li, G. Li, D. Yu, Z. Song, H. Wang, X. Liu, H. Liu, W. Liu, Development of conductive hydrogels for fabricating flexible strain sensors, Small 18 (5) (2021).
[50] J. Kang, S.I. Yun, Chitosan-reinforced PHB hydrogel and aerogel monoliths fabricated by phase separation with the solvent-exchange method, Carbohydr. Polym. 284 (2022).
[51] D.K. Patel, S. Senapati, P. Mourya, M.M. Singh, V.K. Aswal, B. Ray, P. Maiti, Functionalized graphene tagged polyurethanes for corrosion inhibitor and sustained drug delivery, ACS Biomater. Sci. Eng. 3 (12) (2017) 3351–3363.
[52] S. Wang, Q. Liu, M. Li, T. Li, Y. Gu, Q. Li, Z. Zhang, Property improvements of CNT films induced by wet-stretching and tension-heating post treatments, Compos. A: Appl. Sci. Manuf. 103 (2017) 106–112.
[53] G.M. Spinks, S.R. Shin, G.G. Wallace, P.G. Whitten, S.I. Kim, S.J. Kim, Mechanical properties of chitosan/CNT microfibers obtained with improved dispersion, Sensors Actuators B Chem. 115 (2) (2006) 678–684.
[54] F. Sun, H.-R. Cha, K. Bae, S. Hong, J.-M. Kim, S.H. Kim, J. Lee, D. Lee, Mechanical properties of multilayered chitosan/CNT nanocomposite films, Mater. Sci. Eng. A 528 (21) (2011) 6636–6641.
[55] S. Correa, A.K. Grosskopf, J.H. Klich, H. Lopez Hernandez, E.A. Appel, Injectable liposome-based supramolecular hydrogels for the programmable release of multiple protein drugs, Matter 5 (6) (2022) 1816–1838.
[56] J. Liu, J. Garcia, L.M. Leahy, R. Song, D. Mullarkey, B. Fei, A. Dervan, I.V. Shvets, P. Stamenov, W. Wang, F.J. O'Brien, J.N. Coleman, V. Nicolosi, 3D printing of multifunctional conductive polymer composite hydrogels, Adv. Funct. Mater. 33 (2023) 2214196.

[57] D.K. Patel, S.D. Dutta, W.-C. Shin, K. Ganguly, K.-T. Lim, Fabrication and characterization of 3D printable nanocellulose-based hydrogels for tissue engineering, RSC Adv. 11 (13) (2021) 7466–7478.
[58] A.R. Karimi, A. Khodadadi, Mechanically robust 3D nanostructure chitosan-based hydrogels with autonomic self-healing properties, ACS Appl. Mater. Interfaces 8 (40) (2016) 27254–27263.
[59] S.C. Lee, G. Gillispie, P. Prim, S.J. Lee, Physical and chemical factors influencing the printability of hydrogel-based extrusion bioinks, Chem. Rev. 120 (19) (2020) 10834–10886.
[60] S.D. Dutta, J. Hexiu, D.K. Patel, K. Ganguly, K.-T. Lim, 3D-printed bioactive and biodegradable hydrogel scaffolds of alginate/gelatin/cellulose nanocrystals for tissue engineering, Int. J. Biol. Macromol. 167 (2021) 644–658.
[61] M. Chen, J. Tian, Y. Liu, H. Cao, R. Li, J. Wang, J. Wu, Q. Zhang, Dynamic covalent constructed self-healing hydrogel for sequential delivery of antibacterial agent and growth factor in wound healing, Chem. Eng. J. 373 (2019) 413–424.
[62] Z. Ren, T. Ke, Q. Ling, L. Zhao, H. Gu, Rapid self-healing and self-adhesive chitosan-based hydrogels by host-guest interaction and dynamic covalent bond as flexible sensor, Carbohydr. Polym. 273 (2021).
[63] A. Roy Choudhury, pH mediated rheological modulation of chitosan hydrogels, Int. J. Biol. Macromol. 156 (2020) 591–597.
[64] M.-M. Iftime, S. Morariu, L. Marin, Salicyl-imine-chitosan hydrogels: supramolecular architecturing as a crosslinking method toward multifunctional hydrogels, Carbohydr. Polym. 165 (2017) 39–50.
[65] J. Zhang, Y. Liang, Z. Deng, H. Xu, H. Zhang, B. Guo, J. Zhang, Adhesive ion-conducting hydrogel strain sensor with high sensitivity, long-term stability, and extreme temperature tolerance, ACS Appl. Mater. Interfaces 15 (25) (2023) 29902–29913.
[66] S. Dong, S. Feng, F. Liu, R. Li, W. Li, F. Liu, G. Shi, L. Chen, Y. Zhang, Factors influencing the adhesive behavior of carboxymethyl cellulose-based hydrogel for food applications, Int. J. Biol. Macromol. 179 (2021) 398–406.
[67] X. Liu, Z. Ren, F. Liu, L. Zhao, Q. Ling, H. Gu, Multifunctional self-healing dual network hydrogels constructed via host–guest interaction and dynamic covalent bond as wearable strain sensors for monitoring human and organ motions, ACS Appl. Mater. Interfaces 13 (12) (2021) 14612–14622.
[68] J. Park, Y. Lee, T.Y. Kim, S. Hwang, J. Seo, Functional bioelectronic materials for long-term biocompatibility and functionality, ACS Appl. Electron. Mater. 4 (4) (2022) 1449–1468.
[69] M. Selvakumar, S.K. Jaganathan, G.B. Nando, S. Chattopadhyay, Synthesis and characterization of novel polycarbonate based polyurethane/polymer wrapped hydroxyapatite nanocomposites: mechanical properties, osteoconductivity and biocompatibility, J. Biomed. Nanotechnol. 11 (2) (2015) 291–305.
[70] L. Ye, H. Ji, J. Liu, C.H. Tu, M. Kappl, K. Koynov, J. Vogt, H.J. Butt, Carbon nanotube–hydrogel composites facilitate neuronal differentiation while maintaining homeostasis of network activity, Adv. Mater. 33 (41) (2021).
[71] H. Ravanbakhsh, G. Bao, N. Latifi, L.G. Mongeau, Carbon nanotube composite hydrogels for vocal fold tissue engineering: biocompatibility, rheology, and porosity, Mater. Sci. Eng. C 103 (2019).
[72] T. Wang, J. Song, R. Liu, S.Y. Chan, K. Wang, Y. Su, P. Li, W. Huang, Motion detecting, temperature alarming, and wireless wearable bioelectronics based on intrinsically antibacterial conductive hydrogels, ACS Appl. Mater. Interfaces 14 (12) (2022) 14596–14606.
[73] N.A. Mohamed, N.F. Al-Harby, M.S. Almarshed, Synthesis and characterization of novel trimellitic anhydride isothiocyanate-cross linked chitosan hydrogels modified with multi-walled carbon nanotubes for enhancement of antimicrobial activity, Int. J. Biol. Macromol. 132 (2019) 416–428.
[74] Y. Li, C. Chen, L. Han, Z. Lu, N. Zhang, R. Miao, Lignosulfonate sodium assisted PEDOT-based all-gel supercapacitors with enhanced supercapacitance and wide temperature tolerance, Int. J. Biol. Macromol. 254 (2024).
[75] L. Han, Y. Li, C. Chen, Z. Lu, L. Liu, Improved capacitive performance of polypyrrole-based composite hydrogel for flexible self-powered sensing system, Colloids Surf. A Physicochem. Eng. Asp. 678 (2023).
[76] Y. Li, Q. Gong, L. Han, X. Liu, Y. Yang, C. Chen, C. Qian, Q. Han, Carboxymethyl cellulose assisted polyaniline in conductive hydrogels for high-performance self-powered strain sensors, Carbohydr. Polym. 298 (2022).
[77] W. Zhang, X. Zhang, W. Zhao, X. Wang, High-sensitivity composite dual-network hydrogel strain sensor and its application in intelligent recognition and motion monitoring, ACS Appl. Polym. Mater. 5 (4) (2023) 2628–2638.
[78] Q. Li, B. Tian, J. Liang, W. Wu, Functional conductive hydrogels: from performance to flexible sensor applications, Mater. Chem. Front. 7 (15) (2023) 2925–2957.
[79] D. Hardman, T. George Thuruthel, F. Iida, Self-healing ionic gelatin/glycerol hydrogels for strain sensing applications, NPG Asia Mater. 14 (1) (2022).
[80] J. Liu, X. Chen, B. Sun, H. Guo, Y. Guo, S. Zhang, R. Tao, Q. Yang, J. Tang, Stretchable strain sensor of composite hydrogels with high fatigue resistance and low hysteresis, J. Mater. Chem. A 10 (48) (2022) 25564–25574.
[81] P. Du, J. Wang, Y.-I. Hsu, H. Uyama, Bio-inspired homogeneous conductive hydrogel with flexibility and adhesiveness for information transmission and sign language recognition, ACS Appl. Mater. Interfaces 15 (19) (2023) 23711–23724.
[82] G. Ge, Y. Lu, X. Qu, W. Zhao, Y. Ren, W. Wang, Q. Wang, W. Huang, X. Dong, Muscle-inspired self-healing hydrogels for strain and temperature sensor, ACS Nano 14 (1) (2019) 218–228.
[83] T. Xie, F. Ou, C. Ning, L. Tuo, Z. Zhang, Y. Gao, W. Pan, Z. Li, W. Gao, Dual–network carboxymethyl chitosan conductive hydrogels for multifunctional sensors and high–performance triboelectric nanogenerators, Carbohydr. Polym. 333 (2024).
[84] H. Zhang, H. Shen, J. Lan, H. Wu, L. Wang, J. Zhou, Dual-network polyacrylamide/carboxymethyl chitosan-grafted-polyaniline conductive hydrogels for wearable strain sensors, Carbohydr. Polym. 295 (2022).
[85] C. Wang, J. Zhang, H. Xu, C. Huang, Y. Lu, H. Cui, Y. Tan, Chitosan-driven biocompatible hydrogel based on water-soluble polypyrrole for stable human-machine interfaces, Carbohydr. Polym. 295 (2022).
[86] H. Ding, X. Liang, Q. Wang, M. Wang, Z. Li, G. Sun, A semi-interpenetrating network ionic composite hydrogel with low modulus, fast self-recoverability and high conductivity as flexible sensor, Carbohydr. Polym. 248 (2020).
[87] X. Li, X. Li, M. Yan, Q. Wang, Chitosan-based transparent and conductive hydrogel with highly stretchable, adhesive and self-healing as skin-like sensor, Int. J. Biol. Macromol. 242 (2023).